



FINAL PUBLISHABLE REPORT

Grant Agreement number 15SIB07
 Project short name PhotoLED
 Project full title Future Photometry Based on Solid-State Lighting Products

Project start date and duration:		1 September 2016, 36 months
Coordinator: Tuomas Poikonen, VTT		Tel: +358 50 590 4070
Project website address: http://photoled.aalto.fi		E-mail: tuomas.poikonen@vtt.fi
Internal Funded Partners:	External Funded Partners:	Unfunded Partners:
1 VTT, Finland	10 DTU, Denmark	13 INRIM, Italy
2 Aalto, Finland	11 ENTPE, France	14 LMT, Germany
3 CMI, Czech Republic	12 Philips, Netherlands	15 METAS, Switzerland
4 CSIC, Spain		16 OSRAM, Germany
5 Metroserf, Estonia		17 OSRAM OS, Germany
6 BFKH, Hungary		
7 PTB, Germany		
8 RISE, Sweden		
9 VSL, Netherlands		
RMG: -		

Report Status: PU Public

Final Publishable Report

This publication reflects only the author's view and the Commission is not responsible for any use that may be made of the information it contains.



The EMPIR initiative is co-funded by the European Union's Horizon 2020 research and innovation programme and the EMPIR Participating States

TABLE OF CONTENTS

1	Overview	3
2	Need	3
3	Objectives	3
4	Results	4
4.1	LED illuminants and LED reference spectra that can complement or replace the CIE Standard illuminant A (Objective 1)	4
4.2	New LED standard lamps for dissemination and maintenance of the units of luminous intensity, illuminance and luminous flux (Objective 2).....	8
4.3	New photometers and photometric measurement methods that enable illuminance measurement of the new LED standard lamps (Objective 3).....	16
4.4	Reducing the uncertainties of luminous flux and luminous efficacy measurement of solid-state lighting (Objective 4).....	30
5	Impact	34
6	List of publications.....	36

1 Overview

The project addressed the obsolescence of traditional tungsten filament standard lamp technology used in photometric calibrations and the need to support the introduction and uptake of new solid-state lighting (SSL) products. The project developed and validated the basis for a new photometric system based on white light-emitting diodes (LEDs), including new LED illuminants for colorimetry and LED reference spectrum for photometry. New photometric calibration sources and measurement techniques were designed and built, supporting the specific properties of new light sources and detector technology

2 Need

Classical photometry relies heavily on the use of incandescent standard lamps and $V(\lambda)$ -filtered photometers as transfer standards in calibrations of luminous intensity, luminous flux and photometer illuminance responsivity. Photometric measurement methods and spectral data of light sources used in colorimetric analysis of light were established long before SSL products became available for general lighting. Due to the phasing out of incandescent lamps and a lack of the standard lamps (which are used in calibrations) available in the market; a clear and urgent need to develop new LED standard lamps for photometry was identified.

As defined by CIE (International Commission on Illumination), an illuminant is an agreed published spectral power distribution of a theoretical light source, used for analysing reflected or transmitted object colours under specified conditions of illumination. Prior to the start of the project, there were only two illuminants defined as standard illuminants used in photometry and colorimetry for calibration purposes. Due to the introduction and uptake of LED lighting and the disappearance of incandescent transfer standard lamps from the market, there was a need to develop new LED illuminants and reference spectra that are more accurate representations of current lighting technologies.

Luminous flux (lm) and active electrical power (W) of new SSL products are measured in order to determine the luminous efficacy (lm/W) and energy classification of the products. Since spectral responsivities of $V(\lambda)$ -filtered photometers differ from the defined CIE $V(\lambda)$ curve, all photometers are typically calibrated using incandescent light with correlated colour temperature (CCT) of 2856 K. This causes unwanted spectral errors in the measurements of SSL products, as their spectra differ from the spectra of calibration sources. Thus, new LED standard lamps with well-defined spectral power distributions (SPDs) and supporting detector technology are needed to provide convenient and reliable traceability for measurements of SSL products and calibration of photometers to pave the way to lower uncertainties. The objectives of PhotoLED were clearly aimed at addressing the needs mentioned above.

3 Objectives

The overall aim of the project was to develop new technology to replace the phasing-out tungsten filament standard lamps used in classical photometry, and to reduce the uncertainties in luminous flux and luminous efficacy measurements of SSL products by developing new LED standard lamps and supporting detector technology. The specific technical objectives of the project were:

1. To develop LED illuminants and LED reference spectra that can complement or replace the CIE Standard Illuminant A in photometric calibrations and in analysis of colorimetric parameters and to evaluate the consequences of the defined new spectra.
2. To develop new LED standard lamps for dissemination and maintenance of the units of luminous intensity, illuminance and luminous flux triggered by the ban on incandescent lamps. The new LED standard lamps will be optimised for compatibility with existing calibration facilities, spectral properties close to the defined LED reference spectra, well-defined angular uniformity, long lifetime and temporal stability of electrical (DC- or AC-operation), photometric and colorimetric characteristics to enable low uncertainties in measurements of their photometric and radiometric properties.
3. To develop new photometers and photometric measurement methods that enable illuminance measurement of the new LED standard lamps with uncertainties as low as 0.2 % ($k = 2$) in the primary realisation of photometric units, or in calibrations of photometer illuminance or luminous flux responsivities at NMIs, accompanied by high-end spectral irradiance measurement of the new standard lamps with uncertainties as low as 0.4 %.

4. To reduce the uncertainties of luminous flux and luminous efficacy measurement of solid-state lighting (SSL) products at national metrology institutes to 0.5 % ($k = 2$) and to demonstrate that uncertainties as low as 1 % ($k = 2$) can be achieved in a test laboratory.
5. To facilitate the uptake of the measurement methods developed by the project by the measurement supply chain, ensuring traceability of measurement results to the end users (test laboratories, lighting manufacturers) and contribute to the development of standards by the international standardisation committees (CIE) concerning solid state lighting.

4 Results

4.1 LED illuminants and LED reference spectra that can complement or replace the CIE Standard illuminant A (Objective 1)

Classical photometry relies heavily on the use of incandescent standard lamps and $V(\lambda)$ -filtered photometers as transfer standards in calibrations of luminous intensity, luminous flux and photometer illuminance responsivity. Photometric measurement methods and spectral data of light sources used in colorimetric analysis of lighting were established long before SSL products became available in general lighting. Since spectral responsivities of $V(\lambda)$ -filtered photometers differ from the defined CIE $V(\lambda)$ curve, all photometers are typically calibrated using incandescent light with correlated colour temperature (CCT) of 2856 K, corresponding to the CCT of CIE Standard Illuminant A. This method causes unwanted spectral errors in the measurements of SSL products, as their spectra differ from the spectra of calibration sources. Thus, new LED standard lamps with well-defined spectral power distributions (SPDs) and supporting detector technology are needed to provide convenient and reliable traceability for measurements of SSL products and calibration of photometers to pave the way to lower uncertainties. Overall, this objective has been fully met.

4.1.1 Definition of LED illuminants and LED reference spectra

The new LED-based photometric system requires a new LED reference spectrum for calibration use, similar to the CIE Standard Illuminant A that is used as the reference spectrum for incandescent calibration sources in luminous responsivity calibrations of photometers¹. Calibrating a photometer against LED calibration source with a commonly agreed spectrum will reduce spectral mismatch errors, if the photometer is used for measuring similar type of light. Currently, photometers used in laboratories and in the field are calibrated using the CIE Standard Illuminant A spectrum, although more and more LED light is measured. As with Standard Illuminant A, it is beneficial to link the reference spectrum between photometry and colorimetry to enable colorimetric calculations with the spectrum used for calibration of photometers for general light measurements.

During the first year of the project, 1500 spectral power distributions of white LED products were measured and collected from the partners and stakeholders for the analysis of new LED illuminants and LED reference spectra. The white LED spectra that were based on phosphor-converted blue LEDs (BL) were categorised into CCT bins based on ANSI Standard C78.377.2011². The specifications for the chromaticity of Solid State Lighting (SSL) products, provided by ANSI, were also applied to extract outlier SPDs. A total of eight different CCT bins (2700 K, 3000 K, 3500 K, 4000 K, 4500 K, 5000 K, 5700 K, 6500 K) were obtained. Figure 1 represents the repartition of the chromaticities in CIE 1931 chromaticity diagram for the eight CCT bins. The red points represent the 176 outliers that were taken out of the original database for the analysis. Three additional SPDs were excluded from the analysis because of aberrant measurements in higher wavelengths.

¹ CIE 15:2004. *Colorimetry, 3rd Edition*. Vienna: CIE

² American National Standard for electric lamps: Specifications for the Chromaticity of Solid State Lighting Products. Publication ANSI_NEMA_ANSLG C78.377–2008. Rosslyn (VA): American National Standard Lighting Group.

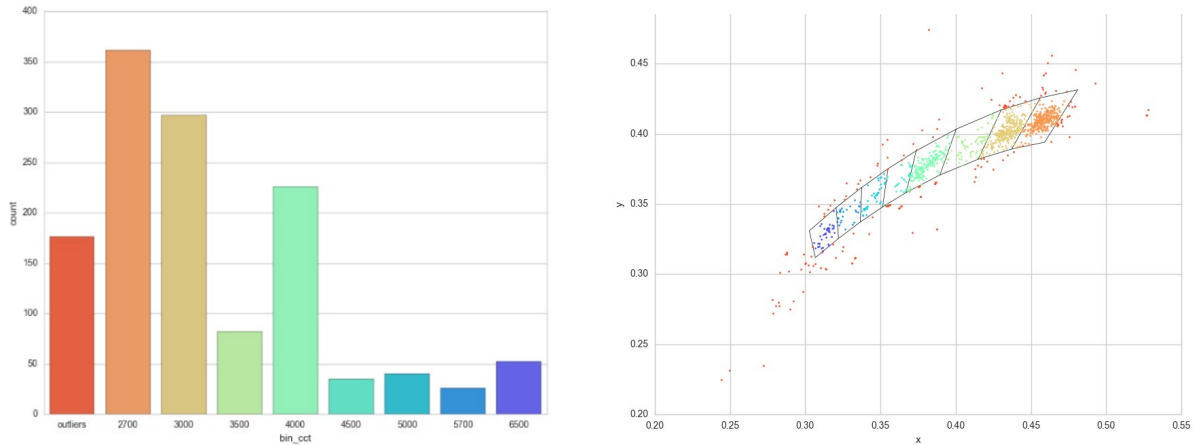


Figure 1. Binning of the LED spectra within the database based on chromaticity.

The typical white LED technologies of the remaining SPDs in the database were identified. In addition, special shapes including blue hybrid (phosphor converted red and blue LEDs), red, green, blue (RGB) and phosphor-converted violet LEDs were chosen as potential LED illuminants for colorimetry.

In order to determine the centroid SPD of each category (bin or technology) the goal was to find the closest SPD to all other SPDs within its category. This was achieved by introducing a closeness score that was defined and calculated for each SPD as

$$C_i^b(S_{zi}(\lambda)) = \sum_{k \in b} 10^{-d(S_{zi}(\lambda), S_{zk}(\lambda))}, \tag{1}$$

where b represents the category, S_{zi} is the i^{th} SPD of the category b and d is any mathematical distance function. This closeness score quantifies with a single number the similarity of each SPD to the other SPDs in the category.

The centroid SPD for each category is the SPD which obtains the highest score. Note that the distance d can be computed in various ways, e.g.:

- 1-Norm distance defined as $d_1(S_{z1}(\lambda), S_{z2}(\lambda)) = \sum_{\lambda=350}^{850} |S_{z1}(\lambda) - S_{z2}(\lambda)|$
- 2-Norm or Euclidean distance defined as $d_2(S_{z1}(\lambda), S_{z2}(\lambda)) = \sqrt{\sum_{\lambda=350}^{850} (S_{z1}(\lambda) - S_{z2}(\lambda))^2}$

1-Norm and Euclidean distances were tested, and as expected, the choice of distance impacts the determination of the centroid. Figure 2 shows this difference for the 4500 K CCT bin and an example of the results obtained for bins of 4 different CCTs. Because the Euclidean distance favors smoother shapes (the RMS function tends to reduce the impact of higher individual features), we decided to use this distance for the analysis.

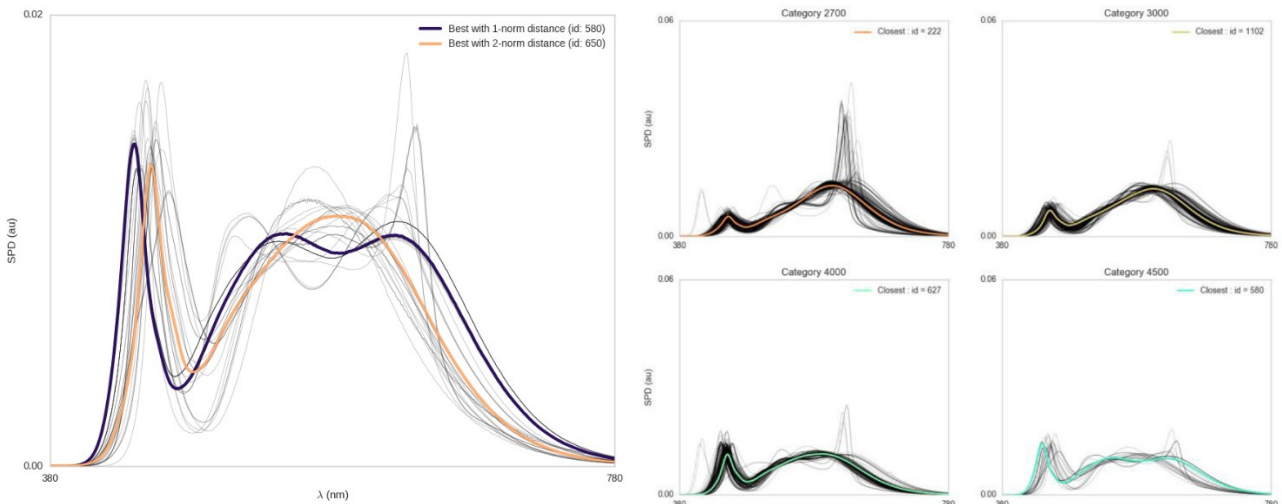


Figure 2. Centroid SPDs for the 4500 K bin, Blue - 1-Norm distance; Red - 2-Norm distance (left) and example of analysis of the representative spectra for bins 2700 K, 3000 K, 4000 K and 4500 K (right).

In order to avoid the issue of recommending a representative LED illuminant of any particular LED manufacturer, but to determine an SPD with feasible spectral features, different methods of averaging were investigated to define a representative illuminant close but different of the centroid, including:

- Averaging the SPDs of n SPDs with the highest closeness scores
- Averaging the SPDs with a closeness score above a fixed threshold
- Averaging the SPDs with a closeness score above a sliding threshold
- Averaging the SPDs of the best closeness scores and the n closest to it

The first three methods lead to averaged SPDs with shapes that might be hard to reproduce, therefore the last averaging method was applied to the SPD with the highest closeness score and the nine SPDs closer to it. Figure 3 represents for the eight CCT bins the centroid SPD (dotted line) and the averaged SPD (full line).

The final step in the analysis for determining the representative illuminants was to clean the data of measurements artefacts. To avoid ripple due to measurement noise, the data was first smoothed by averaging, mainly at low signal levels. Furthermore, bandpass and straylight corrections were applied to the final illuminants based on the information of spectrometers used for the measurements. Finally, the data was extrapolated to the wavelength range of 380–780 nm with 1 nm step.

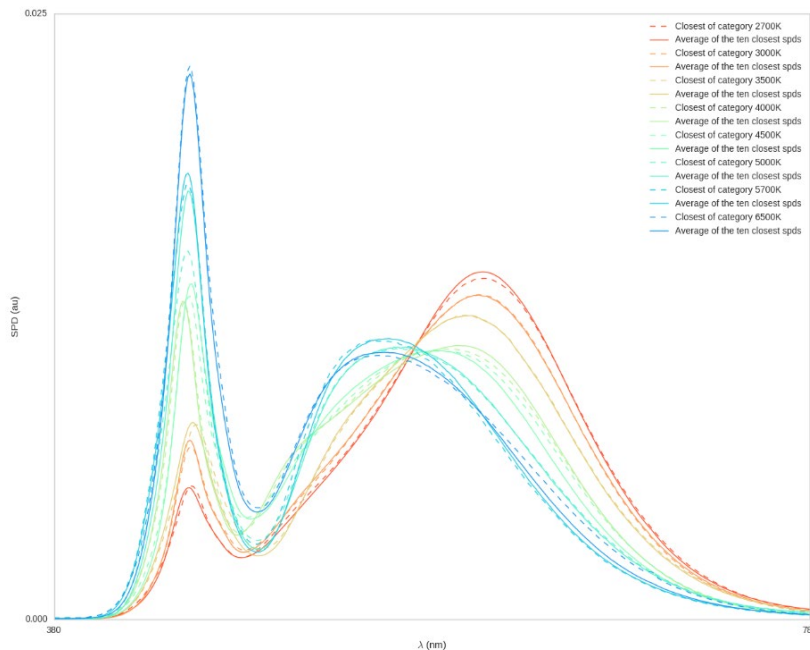


Figure 3. Centroid (dotted line) and averaged SPDs (full line) for the eight CCT bins.

The project submitted the analysed LED illuminants to TC1-85 of CIE Division 1 for consideration to be included as possible LED illuminants in a revision of the CIE Technical Report no. 15: Colorimetry, 4th Edition. The CIE15 document, with the new LED illuminants, was published in October 2018, and is available from CIE. The LED illuminants developed in the project are shown in Figure 4.

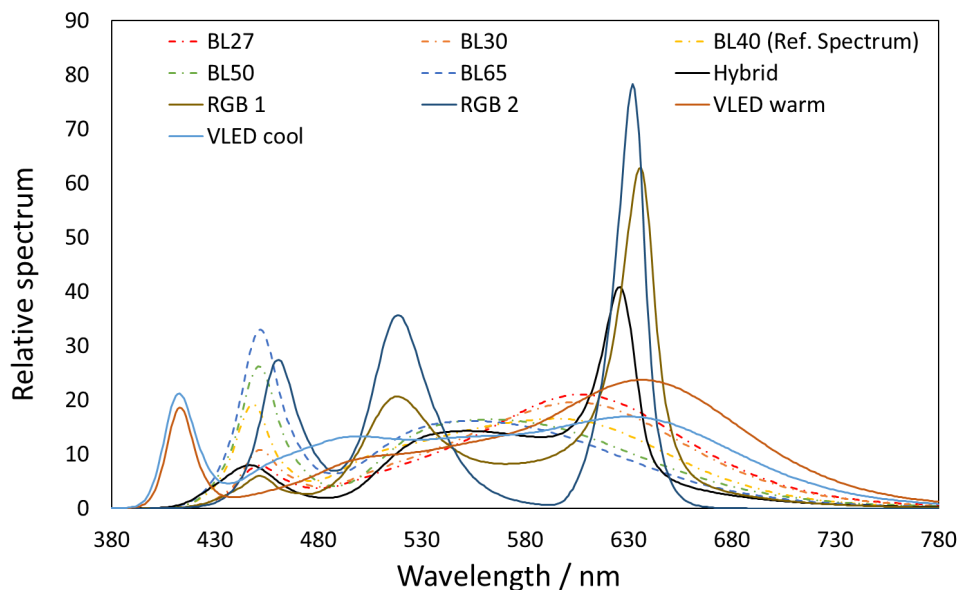


Figure 4. Spectral power distributions of the new LED illuminants developed in the project.

Based on discussions with CIE Division 1 and Division 2, it was found important that the LED reference spectra used in photometry should be a subset of the LED illuminants used in colorimetry. On this basis, the LED illuminants were used as the starting point for analysing suitable LED reference spectra for luminous responsivity calibration of photometers based on which of them would lead to the smallest spectral errors in measurements of light with different SPDs. The analysis was carried out using Monte-Carlo simulation, including calculation of spectral mismatch errors for measurements of the 1500 LED products using the relative spectral responsivity data of over 100 real photometers and SPDs of 8 analysed LED illuminants as possible LED reference spectra. The results showed that a single LED reference spectrum with CCT close to 4100 K would lead to the smallest mean of absolute errors (MAE), when measuring SSL products of different types, reducing spectral errors by a factor of two on average compared to using an incandescent source with the CIE Standard Illuminant A spectrum for calibration of the photometers, see Figure 5.

Using two LED reference spectra would reduce the spectral mismatch errors by a factor of three on average. However, in practical light measurements this would require the end-user to select one of the calibration factors available for example based on estimating the CCT of light being measured. Without carrying a spectrometer, the user would inevitably make selection errors of the calibration factor, losing the theoretical benefit offered by the two reference spectra. This was verified by simulations. Using two reference spectra was discarded at the end, as it did not considerably reduce the spectral errors in practice and would lead to increased complexity and cost of calibrations and measurements. Further tests with the 4103 K LED reference spectrum showed that it led to the smallest spectral errors also in the case of measuring sources other than LEDs, including daylight (C,D), fluorescent (FL) and high-pressure (HP) discharge lamps (Figure 5, right). This analysis was carried out using existing illuminants that have been published in previous CIE Technical Report no. 15: Colorimetry, 3rd Edition. Input was provided from the following project partners: BFKH, PTB, RISE, VTT, DTU, ENTPE, Signify, LMT, METAS, OSRAM, OSRAM OS. The calibration source with 4103 K LED reference spectrum performed best in all cases, except when measuring incandescent light (A) and one type of HP discharge lamp. The detailed results of this spectral analysis were published in A. Kokka *et al.* "Development of white LED illuminants for colorimetry and recommendation of white LED reference spectrum for photometry", *Metrologia* **55**, 526–534 (2018).

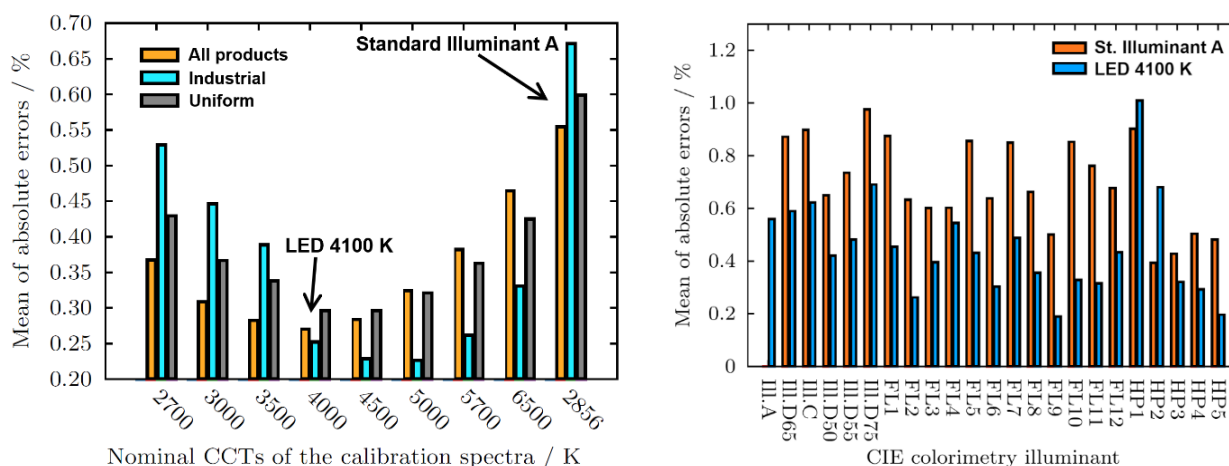


Figure 5. Mean absolute spectral mismatch errors (MAE) obtained in measurements of LED lighting, when calibrating photometers with LED sources having difference CCTs (left) and in the case of measuring other types of light represented by the illuminants of CIE15: Colorimetry.

The influence of the LED reference spectrum on the CIE general $V(\lambda)$ mismatch index f_1' was studied using the different LED illuminants. It was found out that the smallest changes in the calculated f_1' values for photometers can be obtained using the 4100 K LED reference spectrum, as compared to the CIE Standard Illuminant A that is currently used in the definition of the mismatch index f_1' , further supporting the selection of the 4100 K spectrum as an LED reference spectrum. A proposal for an alternative calculation method for the general mismatch index f_1' , including influence of LED spectra in combination with broadband spectra, has been studied and published by A. Ferrero *et al.*, “Index for the evaluation of the general photometric performance of photometers”, *Opt. Express* **26**, 18633–18643 (2018). The results show that it is possible to define an alternative mismatch index which has better correlation between the spectral errors in measurements of light of different types and the calculated f_1' for the photometer. The new mismatch index has been presented to CIE Division 2 for consideration to be taken into use in the future.

Based on this extensive investigation, the project selected the 4100 K LED reference spectrum for selection of suitable LEDs for the new LED standard lamps of the project.

4.1.2 Summary of key research outputs and conclusions

A total of 1500 spectral power distributions of white LED products were measured and collected from the partners and stakeholders for the analysis of new LED illuminants and LED reference spectra. The white LED spectra that were based on phosphor-converted blue LEDs were categorised according to their correlated colour temperatures (CCTs) into 8 different bins between 2700 K and 6500 K. In addition, 4 special shapes including red, green, blue (RGB) and phosphor-converted ultraviolet LEDs were chosen as potential LED illuminants for colorimetry. These illuminants are now included in the revision of the CIE15: Colorimetry, 4th Edition, enabling colorimetric calculations with LED spectra of different types.

The project partners participated in many TCs of CIE Division 2 to ensure that the introduction of new physical LED standard lamps and supporting measurement methods, including the fisheye camera method, are included in these technical documents. In June 2018, a new CIE Division 2 Technical Committee TC2-90 ‘LED reference spectrum for photometer calibration’ was established to further analyse and publish the LED reference spectrum as a CIE Technical Report. In summer 2019, TC2-90 has completed the technical investigation, and the Technical Reports is being written. Once the document is published, commercial LED standard lamps can be manufactured with CIE recommended reference spectrum to complement the Standard Illuminant A in photometer calibrations.

4.2 New LED standard lamps for dissemination and maintenance of the units of luminous intensity, illuminance and luminous flux (Objective 2)

This objective was fully achieved since the project developed new LED standard lamps for luminous intensity and luminous flux. Using the new LED reference spectrum as the basis, suitable LEDs were selected for the new standard lamps using the expertise of the project’s industrial partners. The mechanical, electrical and

optical specifications of the new standard lamps were thoroughly investigated taking into account the typical capabilities of photometric laboratories, while introducing new features, such as thermal control, to take full advantage of the LED technology. The DC-current operated source LIS-A for luminous intensity is aimed at laboratories who require luminous intensity level similar to, for example: Osram Wi41/G incandescent standard lamp. The DC-voltage operated luminous flux standard lamps developed are aimed at laboratories, who look for compact thermally stabilized lamps that can be operated with typical laboratory DC power supplies. AC-voltage operated version of the same luminous flux standard lamp was also developed that can be operated with 230 VAC laboratory power supplies often used by test laboratories. Both sources for luminous flux are aimed at replacing typical luminous flux reference lamps used by laboratories in calibration of photometric system responsivity.

The developed sources offer small spectral errors in measurements of SSL products, reduced signal noise, fast stabilisation, and robustness for transferring the units of luminous intensity and luminous flux between laboratories. The performance of the light sources was validated in two comparisons within the project.

4.2.1 Development of DC-driven white LED standard lamps for luminous intensity and illuminance

The project developed a DC-current driven luminous intensity LED standard lamp LIS-A. The source consists of multiple white LEDs with output aperture and luminous intensity similar to that of a Wi41/G standard lamp. LIS-A can be operated with a laboratory DC current source and an external thermoelectric controller (TEC). A total of 8 standard lamps for luminous intensity were constructed, including seasoning of 1000 h and full characterisation of their luminous intensity, stability and spectral properties. Six of the developed LIS-A sources are shown in Figure 6.

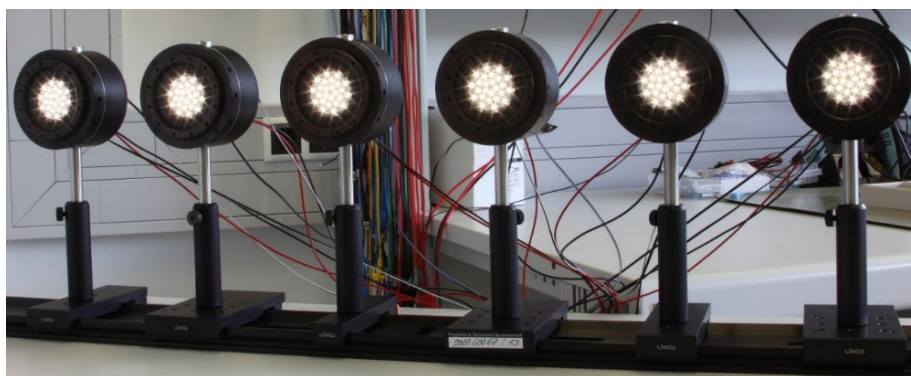


Figure 6. Luminous intensity LED standard lamp LIS-A.

The body of the light source is a black anodized, aluminium cylinder with 100 mm diameter and ~70 mm length. The design allows to stack additional sections to the backside, e.g. to include additional electronics into the housing, without changing the optical properties of the front side. The heating / cooling of the LED-PCB is carried out by a thermoelectric cooler. To ensure stable thermal conditions with low dependency on external air flow the light source is equipped with an internal heat sink and a fan. The air outlet can be directed to the front or sideward. This allows to test different configurations regarding about using the air flow as an air curtain to keep dust away from the LEDs. At the frontside is a ring with inner and outer thread to mount components in front of the light source, e.g. diffusors. Despite having this opportunity, the LEDs will be open to the environment during this first development step because the spectral properties of the LEDs are selected without considering the transmittance of cover glass or diffusor. The outer thread is used to mount an adjustment jig which also acts as dust cover. The electrical connections are available at the backside. The vertical adjustment is supported by a level at the top side. Eight artefacts of this light source were built, six of them with 4100 K LEDs according to the new invented LED reference spectrum / CIE illuminant B3³.

The LEDs are arranged in three rings with 5 respectively 10 LEDs and organized in 5 strings by 5 LEDs each. For the operating current of 0.065 A the lamp voltage is about 71 V for a series connection of all LEDs. For the temperature regulation an internal controller board was implemented. The temperature is measured using a Pt100 resistor, centred on the PCB. The settings of the temperature control can be adjusted by a serial interface and be stored on internal flash memory. So, after configuration of PID parameters and target

³ CIE 015:2018. Colorimetry, 4th Edition. Vienna: CIE.

temperature, the light source can be used without data connection to this internal controller. Only an external switched power supply 12 V/2 A is required for its operation.

One of the reference modules was used for monitoring the aging for about 360 hours. Figure 7 shows the relative change of the LED voltages of each LED string and the relative change of photocurrent of a monitor diode. The data is concatenated from multiple measurement cycles (vertical lines). After 250 hours, the properties get stationary. The measurement cycles show good continuity. Due to test runs before the final characterisation, the reference module got additional operating hours that cannot be determined precisely. To get all modules into a reasonable ageing state, all other modules were aged without monitoring about 1000 hours.

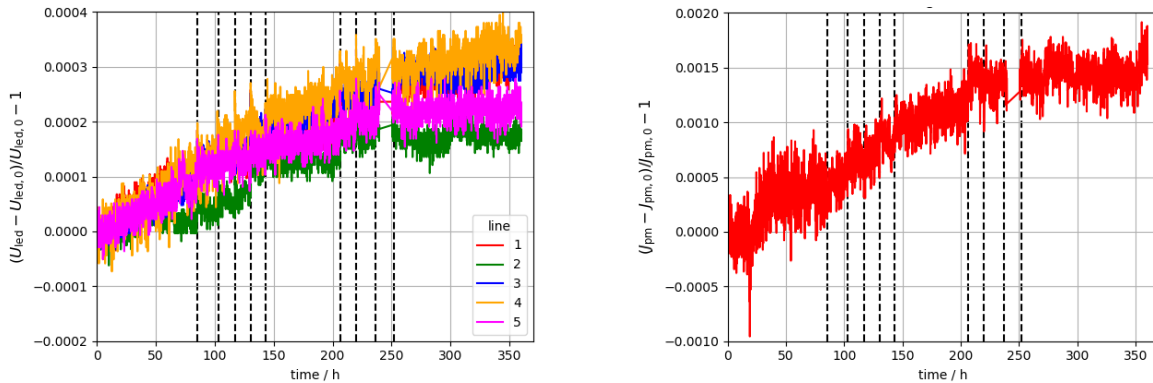


Figure 7. Ageing of reference module, on left is shown the LED voltage and on right photocurrent.

The noise of these ageing measurements is relatively high due to the use of a multi-channel power supply, which does not meet the highest standards. To determine the influence of the ambient temperature and air humidity the light source was operated inside of a climate chamber and monitored with photometer placed outside of the chamber. The temperature was varied between 20 °C and 30 °C while setting the rel. air humidity to 50 %. After 20 min of stabilisation, the photo current was measured. The relative change is below $1.5 \cdot 10^{-4}$ without a common tendency between the light sources and only slightly above the measurements noise level. The stability of the sources was measured using a photometric bench consisting of several detectors. The stability of the electrical operation is in the range of $\pm 1 \cdot 10^{-4}$ for lamp current and $\pm 1 \cdot 10^{-5}$ for the lamp voltage over the 65 hours. The stability of the measured photocurrent is in the range of $\pm 1 \cdot 10^{-4}$, which implies the combined stability of the source’s luminous intensity, photometer, photo-current amplifier and multimeter. This is below the relative standard deviation of about $1.3 \cdot 10^{-4}$. Figure 8 shows the measured spectral power distribution of the LIS-A source. Six LIS-A sources were used in the comparison of luminous intensity that was arranged within the project. More information on the comparison results are presented in Section 4.3.3.

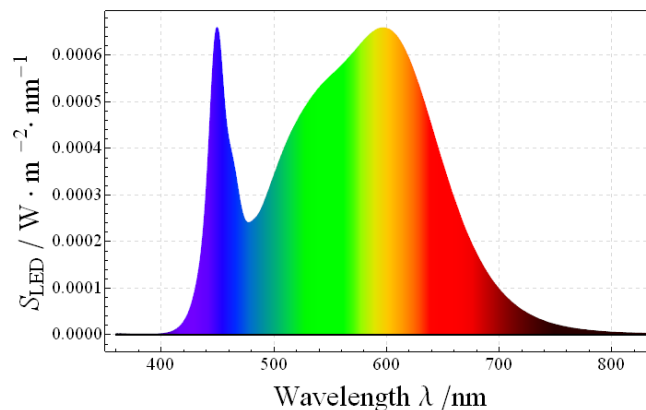


Figure 8. Spectral distribution of one of the LIS-A artefacts.

4.2.2 Development of DC-driven white LED transfer standard lamps for luminous flux

The project developed two types of luminous flux standard lamps with E27-base to ensure compatible with typical integrating spheres and goniophotometers. Both lamps use the same optical design, including LEDs, and produce approximately 800 lm of total luminous flux.

The electronics of the DC-operated lamp consist of a polarity protection circuit, supply voltage filters, linear current source driver for the LEDs, temperature controller, and precision voltage source providing reference to the current source and temperature controller (Figure 9). The electronics are fitted inside a normal retrofit LED-lamp having the shape of a conventional light bulb with a bulb diameter of 61 mm and total length of 107 mm. Constant voltage is provided to the lamp via standard E27 base and no additional wires are required.

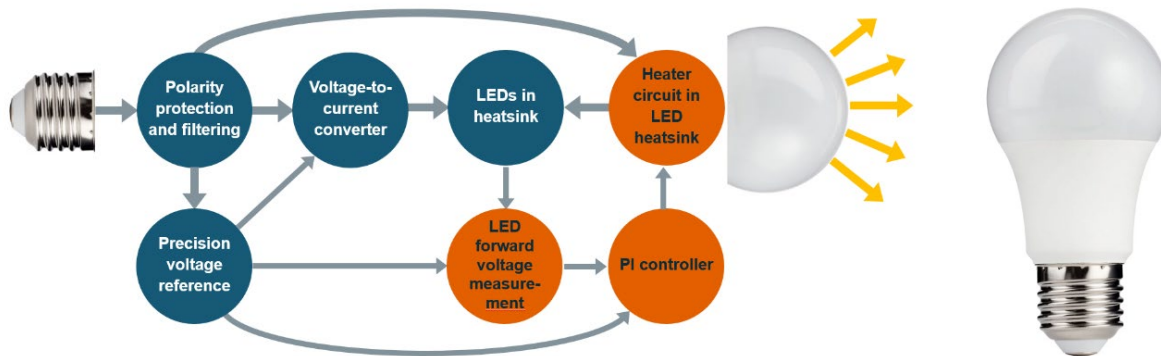


Figure 9. Operational principle and construction of the DC-operated luminous flux transfer standard lamp.

The temperature of LEDs in the lamp is adjusted using a heater circuitry attached to the internal PCB heat sink of the lamp. The circuitry was designed in such a way that the heating power is directly proportional to the control voltage, which is provided by a PI-controller. The lamp temperature is obtained by measuring the voltage over the LEDs that are driven at constant current. This guarantees that the junction temperatures of the LEDs are stabilized rather than the heatsink temperature. Both the LED drive current and the nominal operation temperature can be fine adjusted during the assembly phase to take into account the differences between individual components and the LED chips. Key parameters, such as the time constant of the heating system, were determined, and a Simulink model of the system was used to optimize the PI-parameters.

The quality of the temperature controller was determined by measuring the relative change of luminous flux as a function of ambient temperature. The measurements were performed with and without the temperature controller. In the measurements, the ambient temperature of the room was changed both slowly, utilizing the natural drift of ambient conditions, and rapidly with an air conditioning unit of the room having the on/off cycle of 30 minutes. Results are shown in Figure 10. Five LEDs with CCT approximately 3900 K were used. The lamp is operated with nominal voltage of 16 V DC, leading to approximately 520 mA of current consumption. The total power consumption of the lamp is 6.5 W and it produces 840 lm of luminous flux. The electrical losses of the electronics are approximately 1 W.

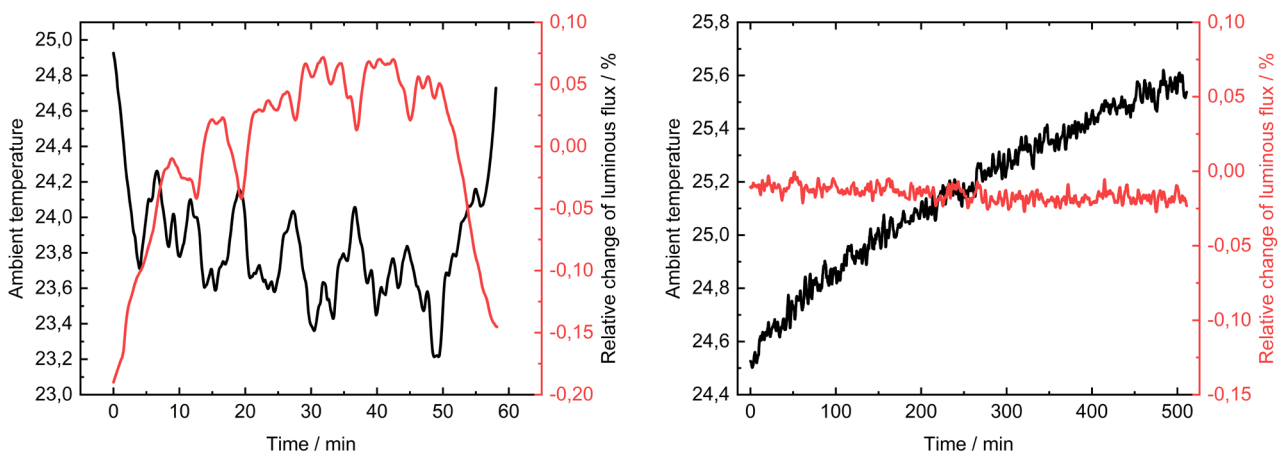


Figure 10. Relative change of flux produced by the lamp, with the TEC disabled (left) and enabled (right).

A total of 6 of the DC-operated luminous flux standard lamps were constructed and characterised, after which they were aged for approximately 1000 hours together with the AC-operated version of the same lamp. The radiometric characterisation results of these lamps are equal to those reported for the AC-operated lamps in

chapter 4.2.3.

4.2.3 Development of AC-driven white LED transfer standard lamps for luminous flux

VSL developed AC-operated LED based luminous flux. The designed lamps (Figure 11) contain five high-power LEDs on a printed circuit board (PCB) with spectral properties selected close to correlated colour temperature of 4000 K, based on the LED-B3 LED reference spectrum⁴. The LED circuit board is covered with a diffuse dome to improve the uniformity of the angular intensity distribution. The LEDs were selected to yield high luminous flux and colour stability. To ensure both constant power consumption from the mains as well as stable current driving the LEDs, an AC/DC LED driver has been developed. The driver was designed to consume more power than needed to drive the LEDs. The excess power makes it possible to regulate both the consumed power from the mains as well as the power (current) needed for the LEDs. Any excessive power is dissipated as heat. The driver was built by combining a rectifier followed by a power factor correcting DC/DC converter. From the stable intermediate DC voltage, a constant current regulator stabilizes the current flowing through the LED PCB to ensure a stable luminous flux and spectral power distribution. Care has been taken to make the circuit insensitive to temperature changes by both selecting components that are temperature insensitive and placement on the PCB away from heat sources. A circuit board with a specific form factor, not to obscure the light emitted from the LEDs, has been developed which contains the LED driver. Furthermore, the components on the circuit board as well as the LEDs are actively cooled with a built-in DC fan. The driver circuit was tested for power consumption with varying load and stabilisation time of consumed power when switching-on the driver.



Figure 11. Mains operated led-based lamp for luminous flux.

RISE seasoned the developed AC-operated LED-based luminous flux lamps. After fabrication, five of the lamps have been seasoned for 800 hours to improve their photometric long-term stability. To maximize the amount of burning hours, while still including possible ageing effects due to on/off-switching, the lamps were burned for 23.5 h each day while being switched off twice for 15 minutes to allow the lamps to cool down. During the seasoning, the temperature of each light source was recorded every 5 minutes with temperature sensor attached onto the top screw heads on each lamp. This position was chosen as it corresponds to the maximum lamp temperature when measured with a thermal camera. At approximately 100-hour intervals the relative luminous flux and the spectral distribution of each lamp were measured using a \varnothing 50 cm integrating sphere equipped with a photometric detector and a fibre optic sensor for spectral measurements using spectroradiometer with TE cooled CCD. The sphere was mounted on a hydraulic lift allowing it to be easily moved between the lamps and accurately positioned for the measurements.

For stability monitoring of the whole setup, another LED lamp with more than 5000 h burn time and verified stability was always measured together with the lamps. Additionally, basic electrical parameters such as RMS current, active power and power factor were monitored at the same intervals. Apart from an initial drop in luminous flux for four of the lamps during the first 150 h, the stability over the seasoning period was within ± 0.2 % for all lamps. This is about the same as the estimated long-term repeatability of the monitoring method, which means that no final conclusions regarding possible small trends can be drawn yet, but the stability for all five lamps are well within what is required for their intended use. A similar drop of luminous flux was observed when seasoning DC-driven LED PCBs with no additional electronics. Also, no significant changes in either electrical parameters nor spectral characteristics have been detected. The seasoned lamps proved to

⁴ KOKKA, A., ET AL., "Development of white LED illuminants for colorimetry and recommendation of white LED reference spectrum for photometry". *Metrologia*, **55**, 526–534 (2018), DOI: <https://doi.org/10.1088/1681-7575/aacae7>.

have a short-term stability better than 0.07 % for power and 0.1 % for luminous flux after 6 minutes and 30 minutes of stabilisation, respectively. After 45 minutes of warmup the luminous flux stability of the lamps improves even further to better than 0.01 %.

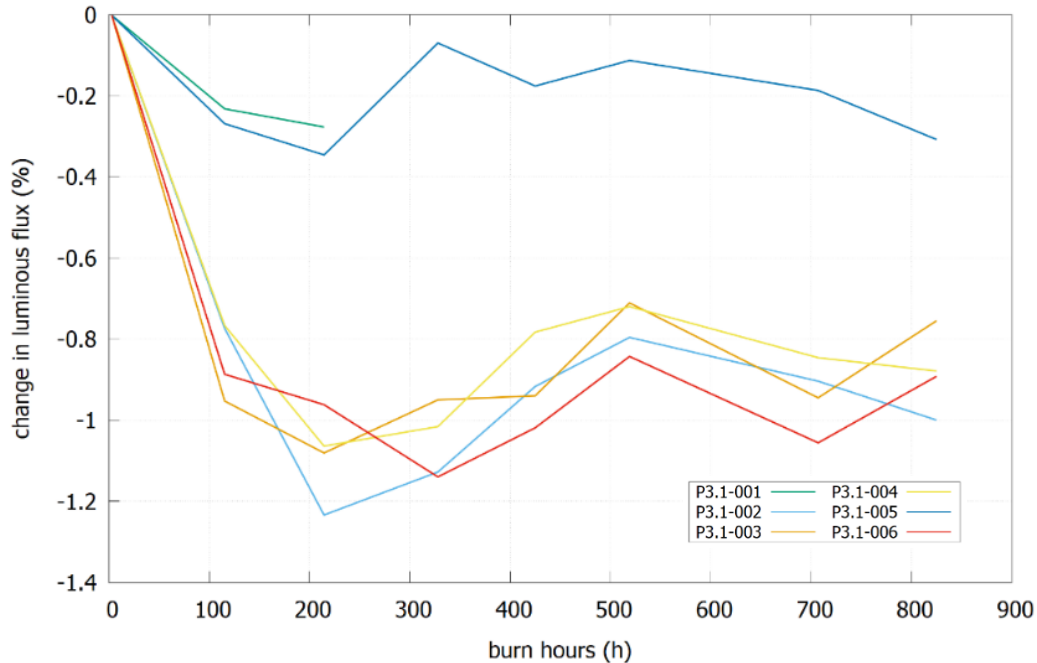


Figure 12. Change in luminous flux during seasoning. Note that one lamp (ID P3.1-001) was removed after 200 h as it was needed for the electronic evaluations.

METAS performed electrical characterizations of the developed AC-operated LED-based luminous flux lamps. One of the built lamps was characterized for electronic performance after 200 hours of ageing. The lamp was mounted in base-up position and powered by a stable 230 V AC-source. During warm-up, the operating voltage, RMS current, active power and power factor were measured. To minimize voltage-drop, the voltage was measured as close as possible to the socket of the lamp. To study the impact of power analyser bandwidth on the measurements, the electrical parameters have been measured additionally by switching the higher corner frequency of the power-analyser from 1 kHz to 2 kHz, 5 kHz, 15 kHz, 30 kHz, 45 kHz, 65 kHz, 75 kHz, 100 kHz, and 300 kHz. The same procedure was repeated using the Impedance Stabilization Network (ISN), developed for the project EMRP Metrology for efficient and safe innovative lighting, [MESaIL](#).

To determine the total harmonic distortion (THD) of the lamp current, a custom-made electrical measurement system for SSL products was used consisting of a stable 230 V AC-source and a digitizer card, developed for the EMRP project [MESaIL](#). During a stabilization time of 35 min all measured electrical parameters showed a stable read out within the required 0.5 % according to the standard CIE S025. Moreover, after 15 min the curves tend to reach a plateau Figure 13. The aim of stabilization time to achieve 0.1 % variation of power is only about 2 minutes, rather shorter than the 45 minutes for typical commercial lamps with consumer grade AC/DC electronics. Furthermore, the demand of a high-power factor for the developed luminous flux standard lamp, to potentially improve the stability of AC voltage supply during measurement, could be achieved as a value of 0.971 ± 0.016 for the power factor was calculated from the measured parameters.

As shown in Figure 14 the impact of different high corner frequency settings of the power analyser to active power, RMS current and the power factor is minor. This means the AC-operated reference lamp performs consistently while operated with different types of artificial mains power sources. In addition, measurement of its power consumption should not be affected by the bandwidth of power measurement equipment used.

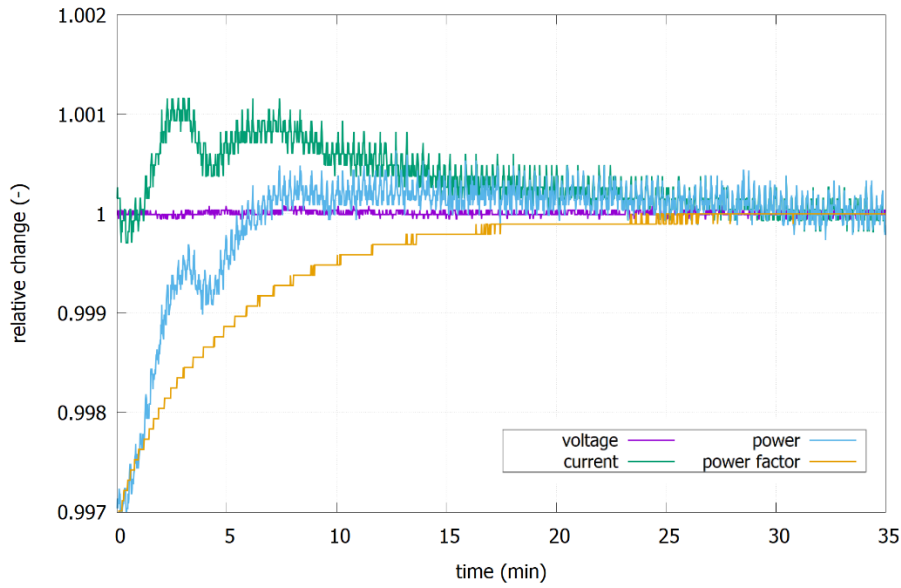


Figure 13. Stabilisation of voltage, current, power and power factor of lamp P3.1-001 after power on.

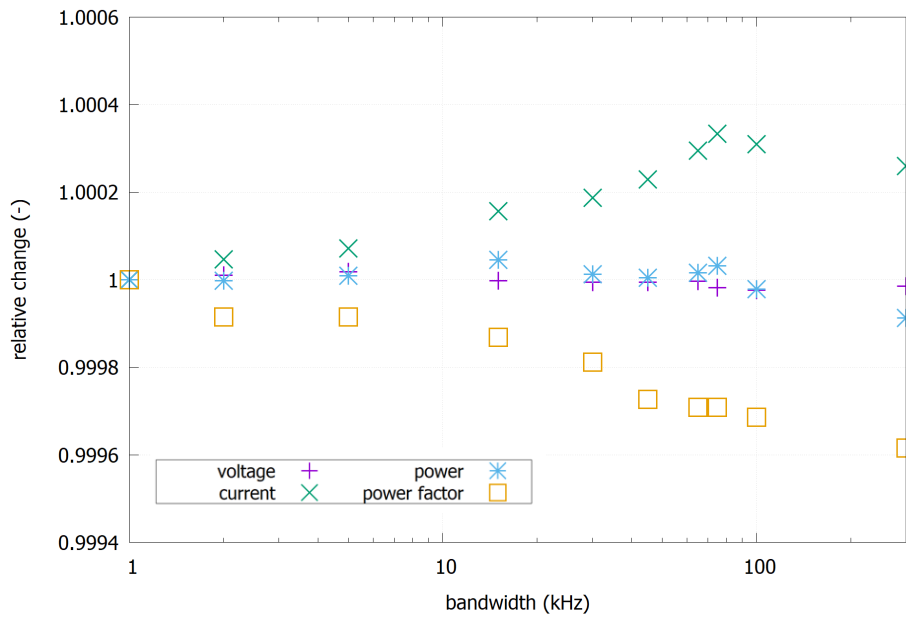


Figure 14. Relative changes of the electrical parameters of lamp (ID P3.1-001) measured with varying bandwidths from 1 kHz to 300 kHz with ISN.

RISE measured the luminous intensity distribution characterizations of the developed AC-operated LED-based luminous flux lamps. To verify that all lamps have similar spectral power distribution and luminous intensity distribution, goniometric measurements were performed using a type C goniometer. These results are needed to achieve the lowest uncertainty when calibrating the total luminous flux of the lamps using an integrated sphere, in order to compensate for sphere non-uniformities and determining the effective spectral distribution when using a PQED in the luminous flux calibration of the sources. For each lamp, the luminous intensity distribution was determined in 1° steps and in six equally distributed c-planes using a photometric detector located 25 m away from the lamp. A similar measurement but in 5° steps was done using a spectrometer with the collecting integrating sphere located about 40 cm from the lamp centre. Due to the lamp design and the used lamp holder, it is estimated that the light emitted backwards (towards the socket) is blocked within ±15°, which should be considered when interpreting the results.

In terms of luminous intensity distribution, as well as the spectral angular distribution, all five evaluated lamps are very similar. As shown in Figure 16, the symmetry around the lamp axes and the c-planes are generally good although with some individual variations and one of the lamps exhibiting an asymmetry of about 10 % for the luminous intensity. However, the influence of this should be negligible in most applications and could be corrected for if needed. In terms of the spectral distribution, all lamps have the highest CCT in the 0° direction (~4100 K). The CCT then slowly decreases towards the sides to about 3900 K at ±160°. The effective colour temperature when integrating the flux over 4π decreases about 100 K compared to the 0° value.

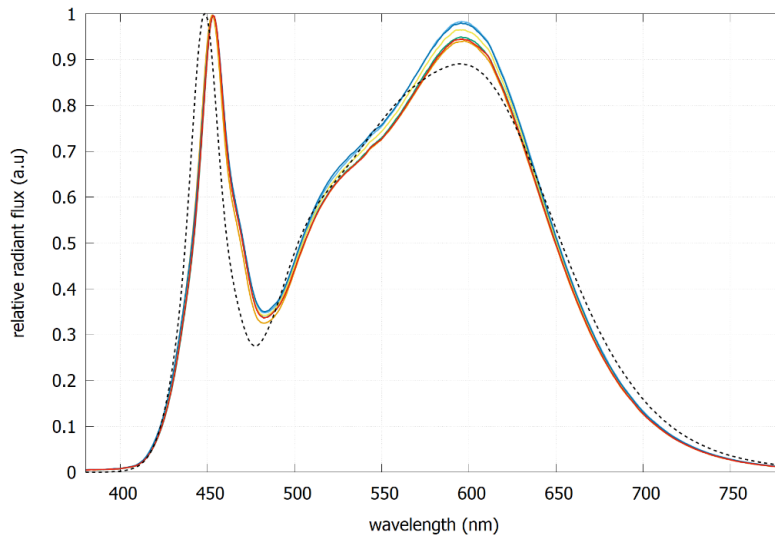


Figure 15. Relative spectral power distributions of the lamps and the reference spectrum (LED B-3).

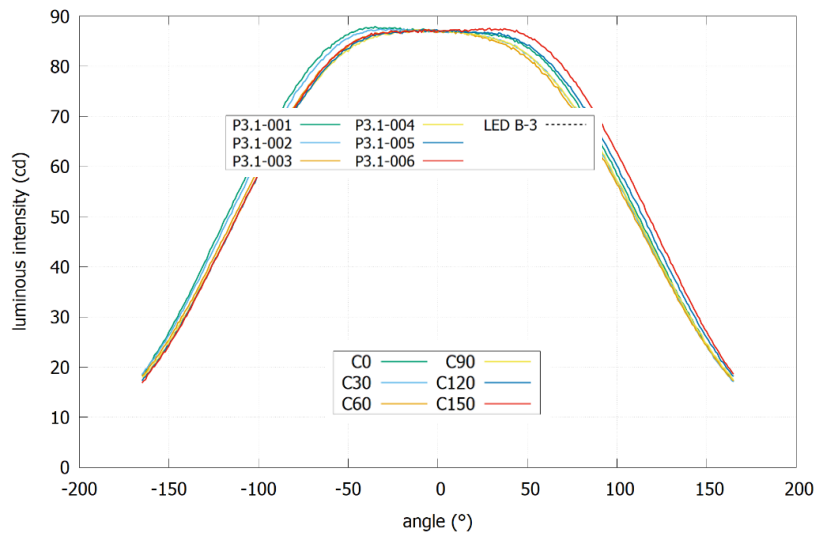


Figure 16. Luminous intensity distribution for lamp P3.1-002.

Full details of this work can be found in:

- P. Dekker *et al.*, 'Mains-operated led-based transfer source for luminous flux scale realisation and dissemination', in *PROCEEDINGS OF the 29th Quadrennial Session of the CIE*, Washington DC, USA, 2019, pp. 1134–1142. http://files.cie.co.at/x046_2019/x046-PO067.pdf

4.2.4 Summary of key research outputs and conclusions

New photometric standard lamps for luminous intensity and luminous flux.

- For luminous intensity, a source LIS-A consisting of multiple white LEDs with output aperture and luminous intensity similar to those of a W41/G standard lamp was developed. The source can be operated with a laboratory DC current source and an external thermoelectric controller (TEC). A total of 8 standard lamps for luminous intensity were constructed, including seasoning of 1000 h and full characterisation of their luminous intensity, stability and spectral properties.
- The project developed two types of luminous flux standard lamps with E27-base to ensure compatibility with typical integrating spheres and goniophotometers. The new lamps produce approximately 800 lm of total luminous flux. Lamp A operates with DC-voltage and includes a built-in precision current source and a TEC. The lamp is optimised for use in a laboratory with 25 °C temperature, as recommended in CIE S025 standard, with ± 4 °C thermal control range. Lamp B operates with 230 V AC voltage and is supplied by an external laboratory AC voltage source. This lamp consists of a constant power AC/DC converter and it is aimed at test laboratories who prefer to calibrate their measurement system without changing the voltage source or wiring. A total of six lamps of each type were constructed, after which they were aged for up to 1000 h, and characterised for electrical, photometric and radiometric properties.

4.3 New photometers and photometric measurement methods that enable illuminance measurement of the new LED standard lamps (Objective 3)

Photometers (luxmeters) are used in the field for measuring illuminance of general lighting and other specific applications. A typical photometer consists of a limiting entrance aperture, an optical $V(\lambda)$ filter and a Si-photodiode assembled in a mechanical enclosure. An ideal photometer would have a spectral responsivity equal to the defined CIE $V(\lambda)$ curve describing the luminous efficiency of the human eye, but even the best $V(\lambda)$ filters available deviate from the ideal $V(\lambda)$ curve, causing spectral mismatch errors in the measurements, which need to be taken into account. In addition, the long-term instability, sensitivity to humidity and fine-structure in spectral transmittance of optical $V(\lambda)$ filters result in major contributions to the uncertainty in the calibration of a conventional photometer. In order to reduce the uncertainties in the calibration of a photometer an improved approach is required whereby the spectral mismatch errors and the influence of the optical $V(\lambda)$ filters are reduced or eliminated.

New photometric techniques and standards based on LEDs are required because traditional incandescent lamps are being phased out and replaced in many every-day lighting applications by solid state lighting (SSL) products, which typically consist of white LEDs. Improved measurement techniques are required for the industry to address the new requirements for traceable, effective and representative measurements and tests for the new SSL products. Primary calibration laboratories are also facing a situation where the incandescent standard lamps currently used as calibration sources in photometry are becoming obsolete and will no longer be available in the future.

This objective has been met, considering the results of the comparison with conventional filtered detectors showed good agreement between laboratories and indicated that the presented calibration methods included all relevant information for corrections and reasonable determination of the measurement uncertainty.

4.3.1 Development of reference photometers

The key parameters were identified for the PQED-based photometers – which were constructed from existing PQED traps – and commercial photodiode photometers – which were then manufactured during the project. The key aspects of the photometers were

- Precision aperture which should be
 - stable, i.e. the aperture area should not change with time due to, e.g., corrosion or accumulation of a layer of contaminant.
 - of good manufacturing quality, in order to make accurate aperture area determination possible.
- Mechanical construction that enables easy alignment of the detector as well as accurate determination of the reference plane.
- Resistance to contamination
 - Nitrogen purging option that can be used during measurements to keep dust away from the photodiodes
 - Sealing option when the photometer is not in use.

- Possibility for temperature monitoring, due to the dependence of the responsivity and dark signal of photodiodes on the temperature.

Based on the design document, three photometers (see Figure 17) based on commercial photodiodes were constructed by Metroser. The three-element reflection type traps used Hamamatsu S1337-1010 photodiodes (active area 10 mm x 10 mm, removable cover windows) in polarization-independent configuration. The photocurrent output is equipped with a BNC connection. Another BNC connector is reserved for temperature monitoring through a 10 k Ω NTC thermistor. The traps are equipped with precision apertures manufactured by CMI. There are M3-threaded holes for dry nitrogen purging valves. However, the valves themselves were not included in the manufactured photometers and were sent to relevant partners by Aalto. The photometers were sent to CMI, CSIC, and PTB.

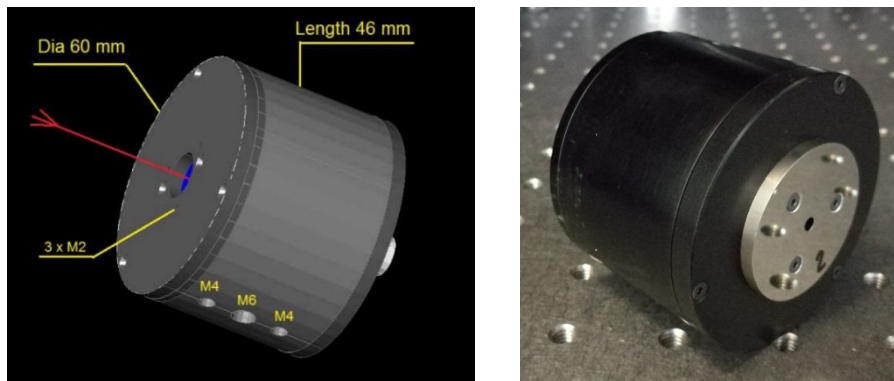


Figure 17. Sketch and photo of the unfiltered photometer manufactured by Metroser. The photograph shows the precision aperture manufactured by CMI.

Figure 18 shows a PQED measuring one of the LED-based luminous intensity sources. PQED-based realization significantly simplifies the traceability chain of photometric measurement results when compared to traditional photometers. This is because there is no need for a cryogenic radiometer and a reference spectrometer to transfer the traceability, as PQED acts as a primary standard for optical power. PQED can be operated at the room temperature, and requires nitrogen flow system, to prevent dust and moisture contamination, and accurate measurement of the relative spectral power distribution of the source in order to apply the spectral mismatch correction.



Figure 18. Predictable Quantum Efficient Detector (PQED) measuring a LED-based intensity source.

The photometers manufactured in were characterized for spectral responsivity by CMI, CSIC, and PTB. CMI characterized the traps using methods A and B, in the wavelength range from 350 nm to 900 nm. In the method A, the aperture of the PhotoLED trap was removed and the spectral power responsivity was measured by CMI

reference spectral responsivity facility. For the measurement setup schematic see Figure 19. The PhotoLED trap was compared against CMI standard trap detector. The measuring beam (convergent f/ #8) under-filled the traps photodiodes. The PhotoLED entrance aperture dimension was measured by optical coordinate measuring machine to get the area, which was used for further calculation of the final spectral irradiance responsivity.

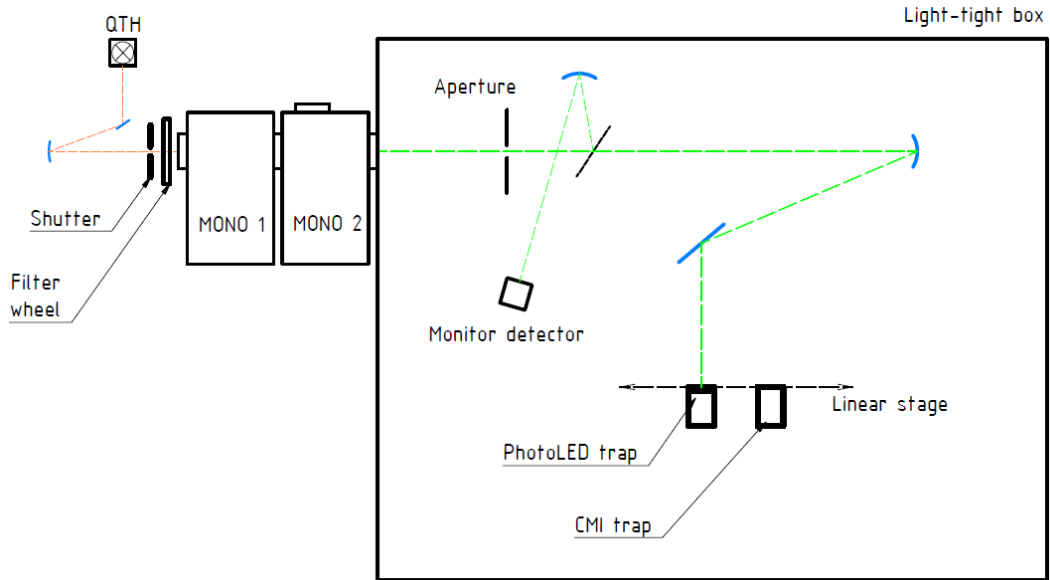


Figure 19: The measurement setup of spectral power responsivity measurement (method “A”) by CMI.

To study if there was any influence of the occasional back reflection to the input aperture the method B was performed. In this case, the entrance aperture of the PhotoLED trap was mounted and the direct spectral irradiance responsivity measurement was done on CMI reference spectral responsivity facility. For the measurement setup schematic of method B (see Figure 20). The front aperture of the PhotoLED trap was over-filled by the measuring beam. The spectral irradiance in the reference plane of the PhotoLED trap detector was alternately measured using CMI standard trap detector and precise calibrated aperture.

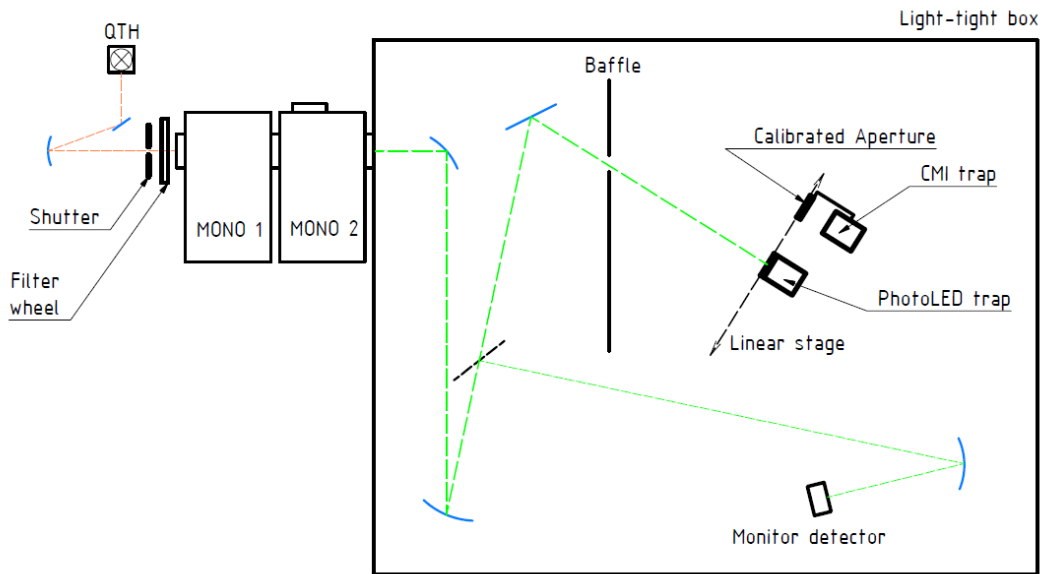


Figure 20. The measurement setup of spectral irradiance responsivity measurement (method “B”) by CMI.

The results of the measurements are presented in Figure 21. The measurement uncertainty was 0.17 % in the spectral range 450 nm – 900 nm, 0.18 % in the spectral range 400 nm – 450 nm and 0.23 % in the spectral

range 350 nm – 400 nm ($k = 1$). The deviations of the results given by these two methods (A,B) were lower than the measurement uncertainty (see Figure 22). It confirmed the negligible influence of the back-reflections of the front aperture of the PhotoLED trap, which were expected during the first measurement technique.

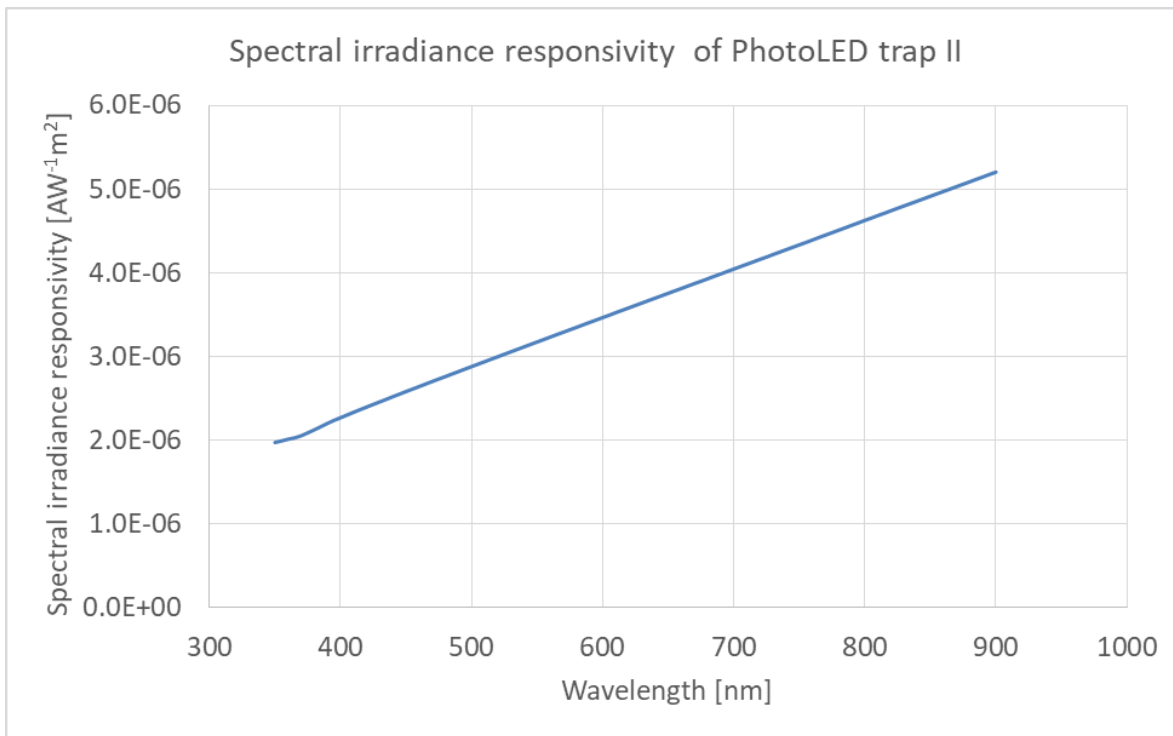


Figure 21. Spectral irradiance responsivity of one of the unfiltered photometers characterized by CMI.

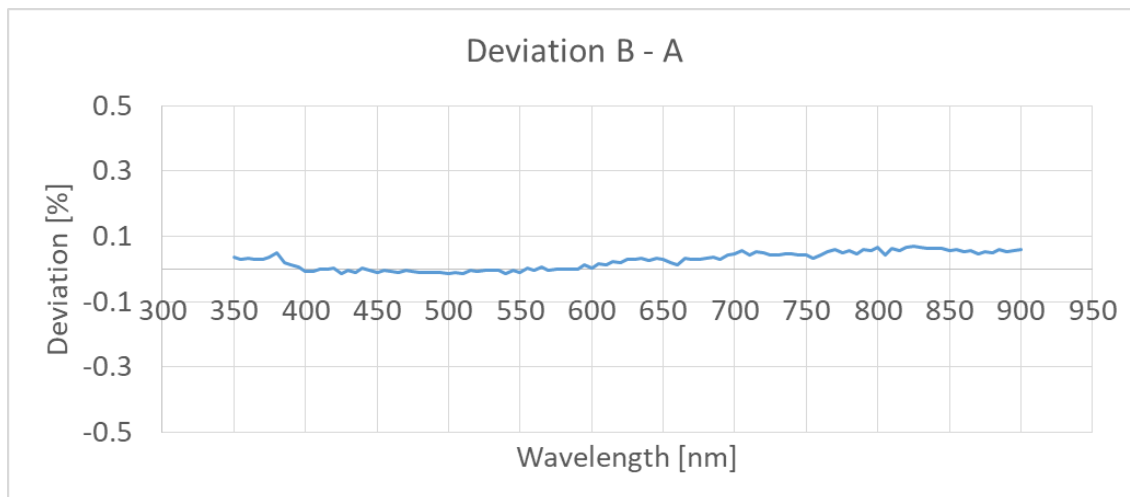


Figure 22. The relative deviation of the two methods B-A of CMI.

CSIC characterized the traps using two single-grating monochromators: one for the UV range with a Xe-Hg source and one for the Vis-IR range with a quartz tungsten halogen (QTH) source, in the wavelength range from 350 nm to 950 nm. PTB characterized the traps using a tuneable laser system in the wavelength range from 340 nm to 940 nm. Results of the PTB measurement are shown in Figure 23.

During the measurements of the spectral responsivities of the trap detector-based photometers without a $V(\lambda)$, it was noted that the photometers unexpectedly picked up AC interference which could limit the accuracy of the measurements especially when measuring low photocurrents. To combat this issue, Metroserf suggests

that the user unscrews one of the screws from the back panel and replaces the screw with a non-anodized screw. This screw can then be used as a terminal for grounding the housing of the photometer.

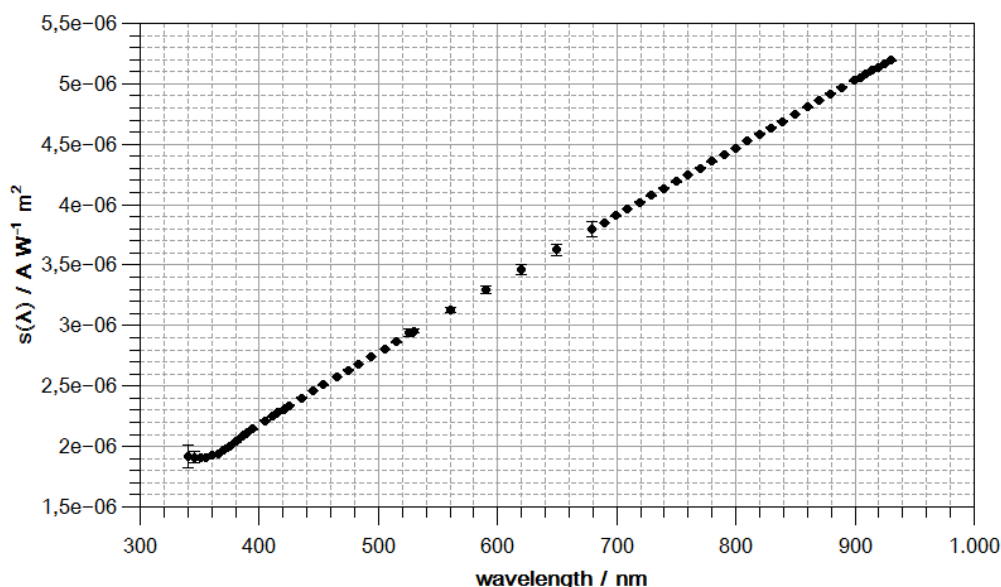


Figure 23. Spectral responsivity of one of the unfiltered photometers characterized by PTB.

Six precision apertures (see Figure 24) were designed and manufactured by CMI, three for PQED photometers and three for commercial photodiode traps. For the PQED apertures, the diameter for the opening was 4 mm, whereas 3 mm opening was selected for commercial photodiode traps. The apertures were manufactured from stainless steel and produced by CNC machining. Final surface finishing was done to improve surface circularity of the aperture. After the initial characterization, an additional surface treatment step was taken to improve the quality of the edge of the aperture. This enables more accurate aperture area characterization.

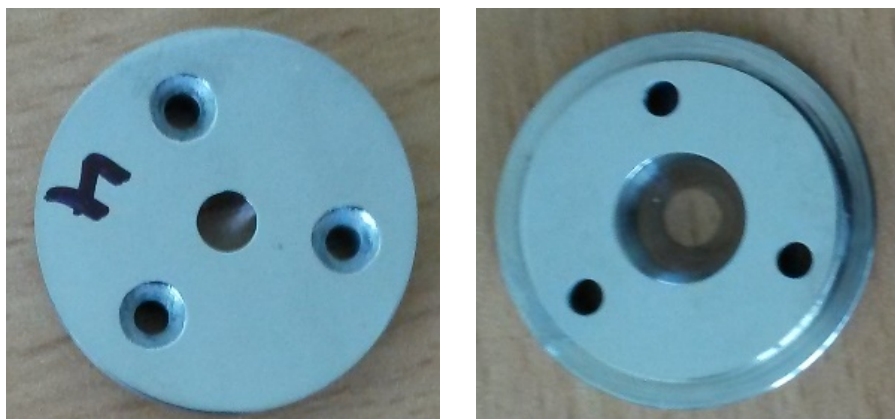


Figure 24. The 4 mm aperture manufactured by CMI.

Aalto designed and built an optical aperture area measurement system that does not require the removal of the aperture from the detector. The aperture area is measured by utilizing a superposition of equally spaced Gaussian laser beams that forms uniform and known irradiance distribution. In practice, this is accomplished by scanning the aperture and detector assembly in front of an intensity-stabilized laser beam. The length scale of the translational stages was calibrated by VTT using laser interferometry. The aperture area can be determined from the measured photocurrents at different translator positions and the photocurrent produced by when the laser beam is not obstructed by the aperture.

The preliminary results of the aperture area measurements are shown in Figure 25. For comparison, the area of the aperture was also measured with traditional coordinate-measuring machine-based methods at CMI and

VTT before it was attached to the PQED. The uncertainty of the area determined with the new method is dominated by the length scale of the translational stages and reproducibility of the measurements.

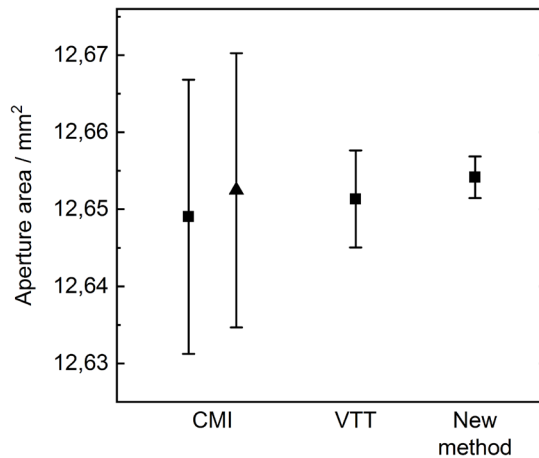


Figure 25. Area of a 4 mm aperture determined with optical coordinate-measuring machines (CMMs) at CMI and VTT, and with the new method. The CMI calibration gives two values, one obtained from the CMM directly (triangle) and another calculated from the raw data (square).

4.3.2 Calibration of spectroradiometers for the characterisation of relative spectral irradiance of the white LED standards

Photometry of LED transfer standards requires knowledge of their spectrum, i.e., the relative spectral irradiance produced by the LED. Such information is usually obtained with the help of array spectroradiometers. To obtain high-accuracy results, array spectroradiometers must be characterised for a number of important instrumental properties. This document describes characterisations of the instruments with respect to spectral stray light, bandpass functions, wavelength-to-pixel assignment and linearity. The characterised spectroradiometers were used by PTB within the PhotoLED project to measure the developed white LED standards.

Spectral characterisations of array spectroradiometers at PTB included determination of line spread functions (LSF), which contain information on stray light and bandpass properties, throughout the spectral range of the instrument as well as the pixel-to-wavelength assignment. The measurements of these properties were carried out using a spectrally tuneable laser setup based on a nanosecond optical parametric oscillator (ns-OPO, see Figure 26). The wavelength of the tuneable laser source was monitored with an uncertainty of 3 pm using a wave meter (laser spectrum analyser) and a high-resolution spectrometer. The known wavelength of the laser radiation was taken as the basis for a pixel-to-wavelength assignment. The linearity characterisation was accomplished by irradiation with a continuous-wave laser radiation and a comparison to a linear silicon detector.

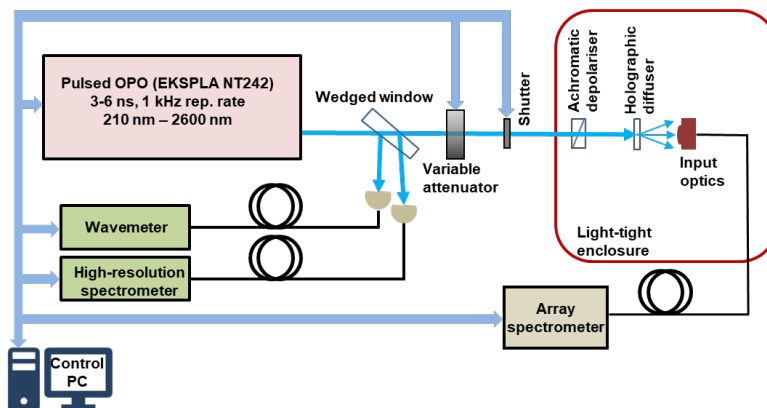


Figure 26. Tuneable laser setup used for spectral characterisations of array spectroradiometers at PTB.

Stray light and bandpass properties of an array spectroradiometer are fully described by so-called line spread functions (LSF) that provide spectral response of the instrument to a monochromatic irradiation with a wavelength within its spectral range. Optical radiation with wavelengths outside the spectral range of the spectroradiometer can cause so-called out-of-range stray light. This stray light cannot be described by the LSFs and requires other methods to be involved. For the array spectroradiometers used for the LED measurements in the PhotoLED project, only the in-range stray light properties were important, which were considered by the measured LSFs.

The measured LSFs of one of the CCD-array spectroradiometers selected for LED measurements are shown in Figure 27. The figure shows a moderate stray light level for most of the spectral range. For laser wavelengths concentrated at around 700 nm satellite peaks are observed, which increases the near-field stray light and has an effect on the wavelength calibration. Figure 28 presents a close-up of LSFs normalised to the peak pixel at several laser wavelengths, showing a change of shape of the slit functions throughout the spectral range of the spectroradiometer. Figure 29 present wavelength dependence of the full-width at half-maximum (FWHM) of the spectroradiometer bandpass functions. In Figure 30, difference between the centroid and peak pixel is plotted as calculated from the LSFs, which demonstrates that not only the width of the bandpass functions but also their asymmetry are changing with wavelength, as there would be no difference between the centroid and peak values in the case of symmetrical bandpass functions.

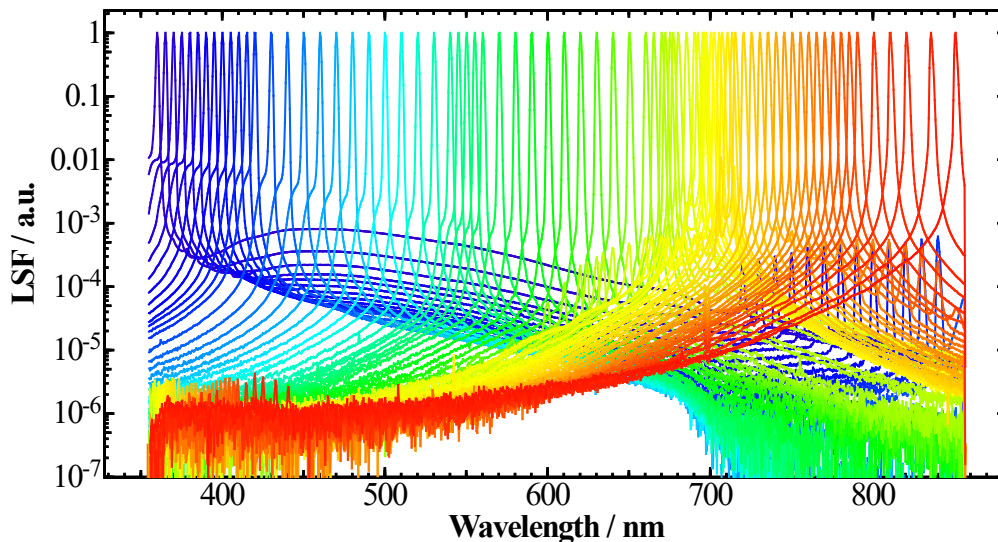


Figure 27. Line spread functions (LSF) of an array spectroradiometer selected for LED measurements.

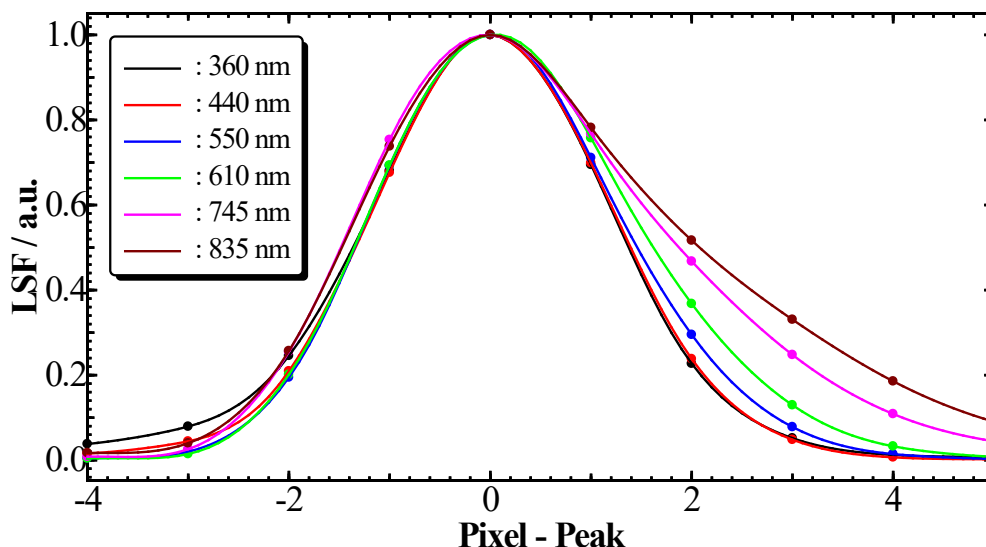


Figure 28. In-band region of several LSFs normalised to peak value and peak pixel.

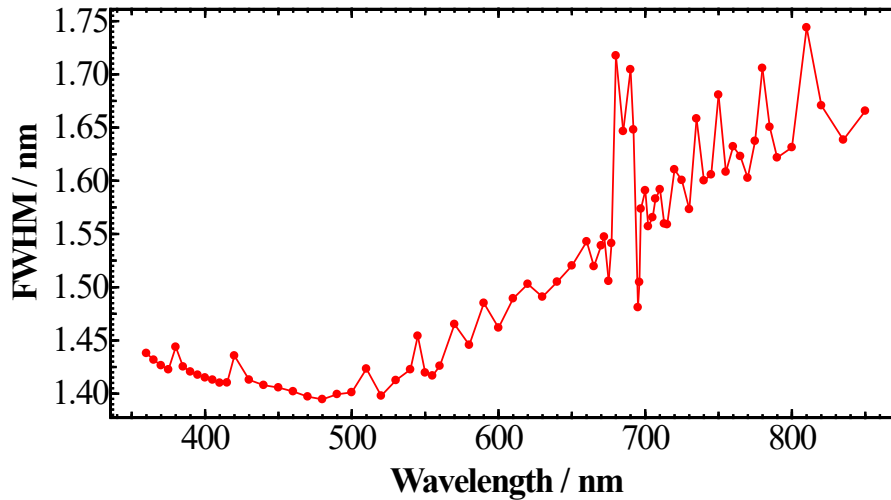


Figure 29. Change of the bandwidth (FWHM) with wavelength.

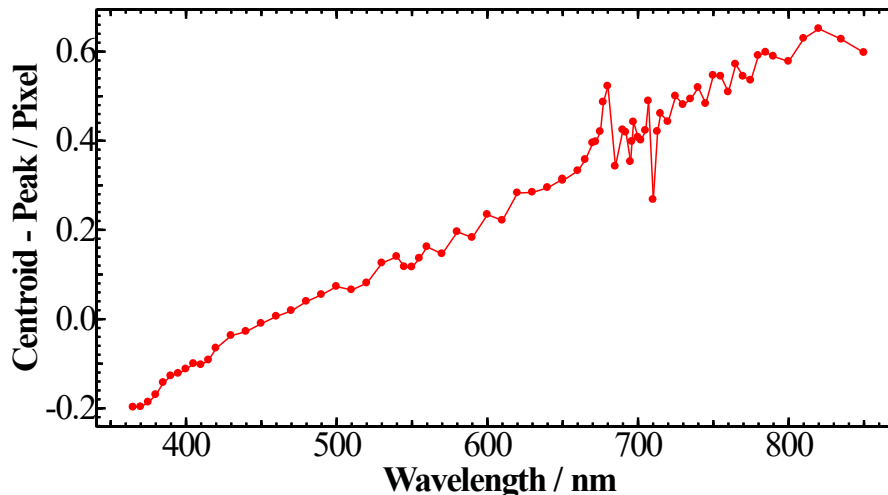


Figure 30. Difference between the centroid and the peak pixels, which shows the variation asymmetry of the slit functions with wavelength.

Pixel-to-wavelength assignment: conventional approach

For wavelength scale calibrations of spectroradiometers, typically lamps with atomic emission lines (Hg, Ar, Cd, etc.) are used. The measured spectral peaks are compared to the known wavelengths of the lines, which are provided. This calibration approach is widely used since the atomic emission lamps are cost-efficient and commercially available. The disadvantage is that a set of many lamps is required to generate a dense grid of data points covering the wavelength scale of the spectrometer. Moreover, not all lines may be suitable for the calibration because some of them are too close to each other and some of the lines are even within the bandpass of the spectrometer, which makes the assignment of the peak wavelength complicated.

Fabry-Perot etalon-based calibration

The inaccuracy of the pixel-to-wavelength assignment of a spectrometer can be found in a fast way by using a Fabry-Perot etalon. A Fabry-Perot etalon consists of a cavity formed by two partially transmitting mirrors in a plane parallel configuration at a given separation distance. The transmission of a Fabry-Perot etalon shows a specific resonance pattern with given wavelength peaks. The resonant wavelengths depend on the design of the Fabry-Perot, mainly the optical properties of the mirrors and the length of the cavity. The transmission spectrum of a Fabry-Perot etalon can be modelled, if these parameters are known precisely. This is shown in Figure 31, where the simulated pattern is in black.

The transmission of the Fabry-Perot can be measured with a collimated beam of a light source having a broadband spectrum. In this case, a halogen lamp is used. The measured positions of the resonance wavelengths depend on the pixel-to-wavelength assignment of the spectrometer. The differences between the measured positions and the known position of the modelled Fabry-Perot etalon are computed for each wavelength, as shown in the image on the left of Figure 31. Those differences are used to fit a polynomial to approximate the pixel-to-wavelength assignment function of the spectrometer. The polynomial fit used has a degree of nine. The lines of an HgAr lamp with known peaks are also measured to have some supporting points where the wavelength is defined by the physical properties of the gas in the source. One line of the HgAr measurements is used in the algorithm to find the accurate spacing between the two mirrors by an optimization algorithm. This is required, as the length of the Fabry-Perot cavity is only known from the theoretical mechanical design with a low precision.

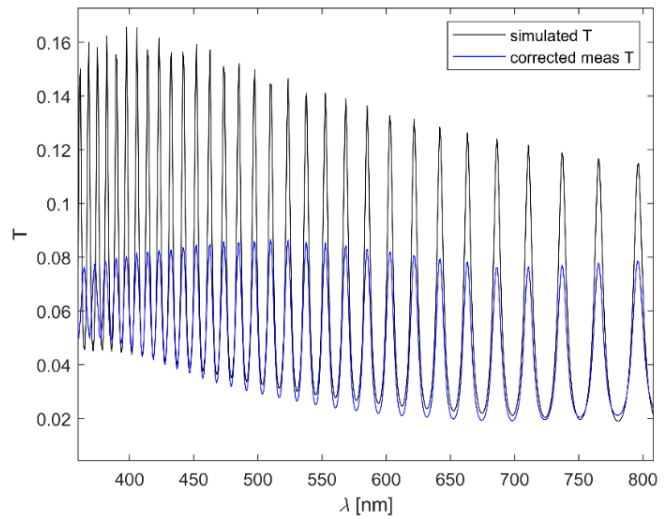


Figure 31. Simulated (black) and measured (blue) transmission spectrum with a Fabry-Perot etalon. The measured spectrum is shown after the correction with the polynomial fit.

The HgAr wavelength chosen as fitting point is 738.398 nm. Once the polynomial is determined, the correction can be applied to the spectrum (blue curve in Figure 31). The difference in amplitude is due to the slit function of the spectrometer. The residual errors after correction with the polynomial are then computed, as shown on the right side of Figure 32. Some measurements are acquired with a tunable laser and a high-resolution spectrometer in order to validate the results from the Fabry-Perot etalon. The two sets of measurements show a good agreement. The residual errors after the polynomial fit are within ± 80 pm for the Fabry-Perot and the HgAr measurements.

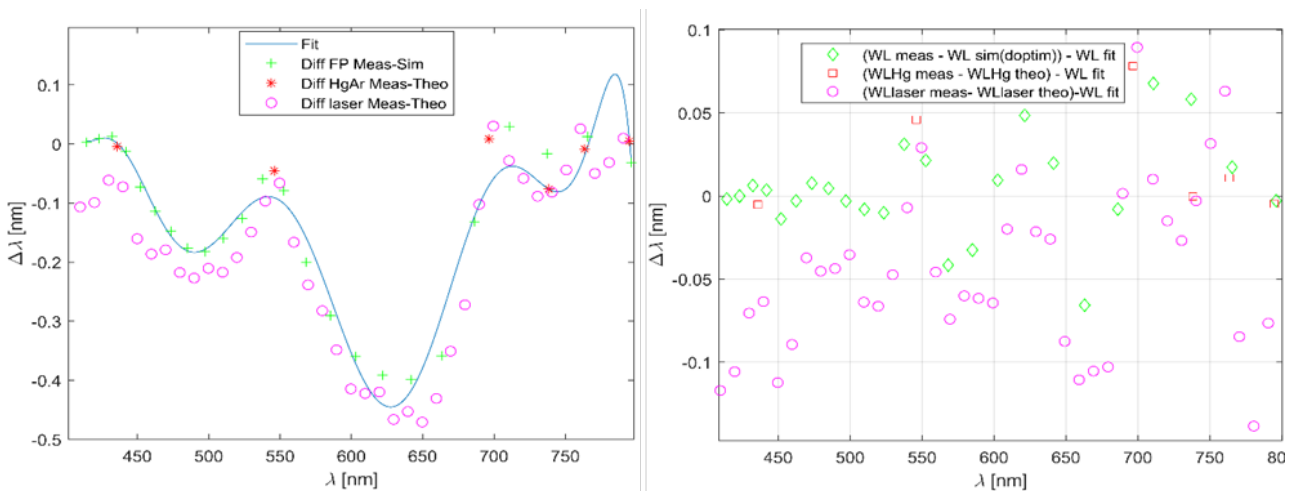


Figure 32. Left: differences between the measured wavelength positions and the theoretical wavelength positions with the Fabry-Perot (green), the HgAr lamp (red) and the tunable laser (pink). Right: corresponding residual errors after the correction of the pixel-to-wavelength assignment of the spectrometer with the polynomial.

Tuneable laser and wavemeter-based calibration

For a perfect spectrometer, a pixel-to-wavelength assignment of a spectroradiometer can be approximated by a simple function, e.g. a low-order polynomial. In practice, it is not only the dispersion function of the grating spectrometer, which affects this function. It is contributed also by other features of the spectrometer, such as optical aberrations, multiple diffraction, interreflections from the optical components, etc. As a result, the line spread functions or the slit functions, more specifically, become non-symmetric and changing throughout the spectral range of the spectrometer. Often also local modulations of the slit function, such as splitting of the peak or appearance of pronounced side peaks close to the main peak, can be observed in certain wavelength ranges. All this requires mapping the pixel-to-wavelength assignment on a narrow grid and makes it difficult to approximate by a function with low residuals. Under this aspect, measurements using a narrowband tuneable laser source and a wavemeter offers a great advantage as this allows to get a dense grid of data points for accurately mapping the specific pixel-to-wavelength assignment function of a spectroradiometer.

It is important to note that the choice of the method for the peak detection affects the wavelength calibration of spectroradiometers having non-symmetrical bandpass functions, which is typically the case for array spectroradiometers. To achieve the best results it is recommended to use the centroid values of the spectral peaks rather than the maximum of the peak values for the assignment of the peaks. We refer to the expression for the centroid of the bandpass-peak, which is given as a ratio of two integrals,

$$\lambda_c = \frac{\int \lambda \cdot LSF(\lambda) d\lambda}{\int LSF(\lambda) d\lambda}. \quad (1)$$

As array spectroradiometers typically have non-symmetrical bandpass functions and are affected by near-field stray light, the integral values may be noticeably dependent on the choice of the lower and the upper limits, which can be expressed as $\lambda_0 \pm N \cdot FWHM$, for integrating the functions in nominator and denominator of (1). The choice of the limits, hence, depends on the individual LSF shape. However, the required integral limits are reduced and well defined in case the stray light correction matrix is applied. As an example, Figure 33 demonstrates the effect of the stray light correction matrix applied to an LSF. Figure 34 shows the centroid value of the peak determined under different integration limits, from $-N \cdot FWHM$ to $N \cdot FWHM$. Here one can see that the value of the peak pixel determined as the centroid of the LSF becomes constant only after the integration limit is about $N = 10$ times the $FWHM$ to both sides of the peak. For the stray light-corrected LSF , a stable value is reached already at $4 \times FWHM$, as the near-field stray light is effectively removed by the correction.

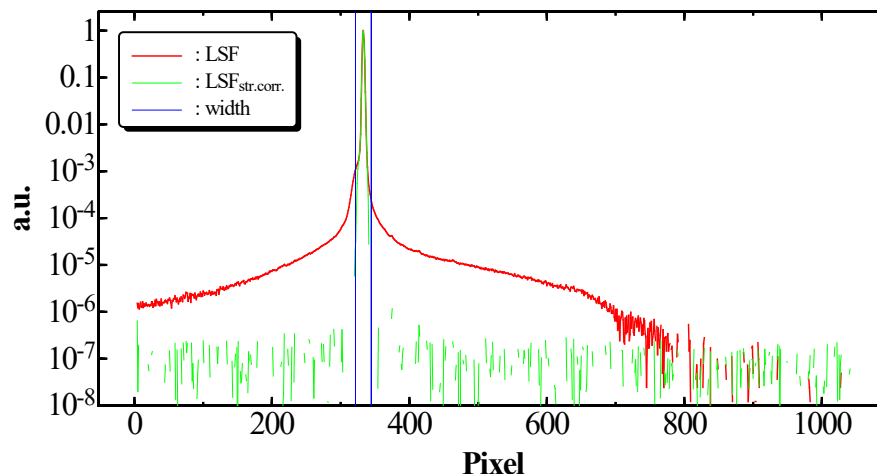


Figure 33. Effect of the stray light correction matrix applied to an LSF.

The determined pixel-to-wavelength assignment of the array spectroradiometer is shown in Figure 35. The values were fitted by a 4th order polynomial with residuals of the fit being at the level of 0.02 nm for most of the spectral range. For the wavelengths in the spectral range around 700 nm, the residuals are higher. It must be noted that the increase of the residuals is not because of a laser wavelength stability or of other stochastic origin. They are a result of side peaks biasing the slit functions in this wavelength region. Rapid changes of the slit functions thus increase the uncertainty of the function values assigning pixels to wavelengths (see Figure 36).

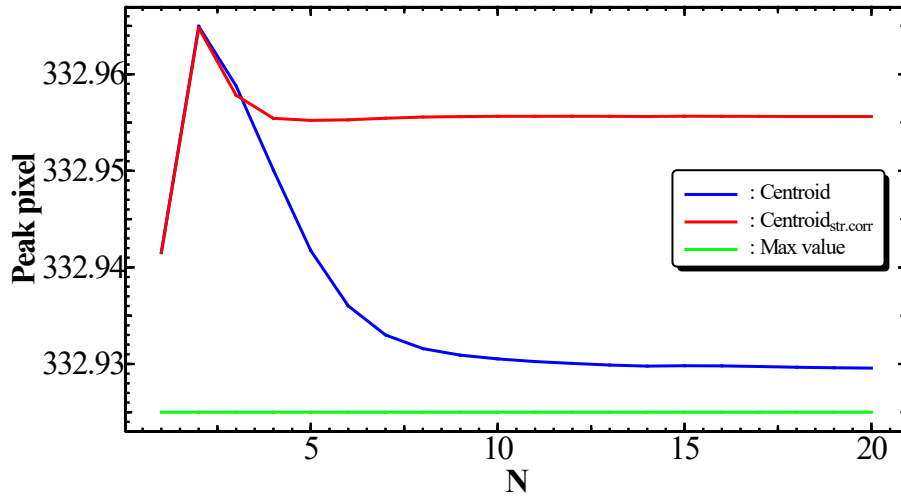


Figure 34. Peak pixel value determined as a centroid of the LSF with and without stray light correction integrated over $\pm N \times FWHM$. The determined centroid value does not change for $N \geq 4$.

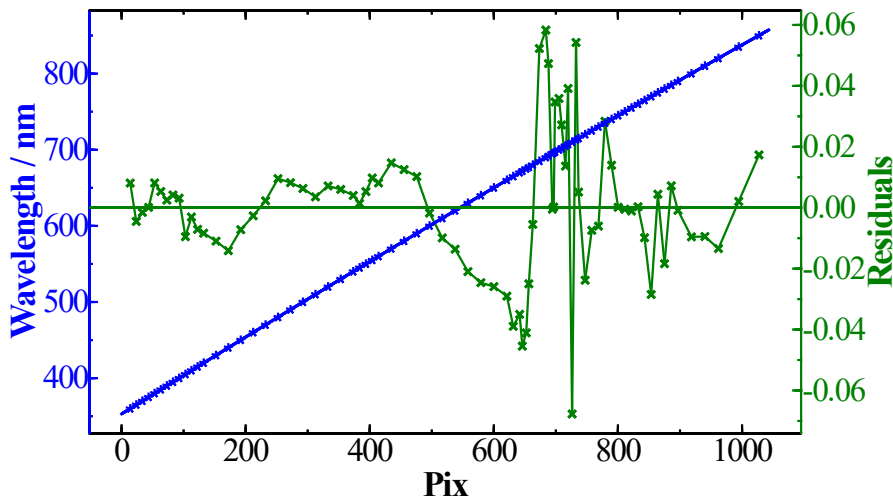


Figure 35. Pixel-to-wavelength assignment of the array spectroradiometer fitted by a 4th order polynomial.

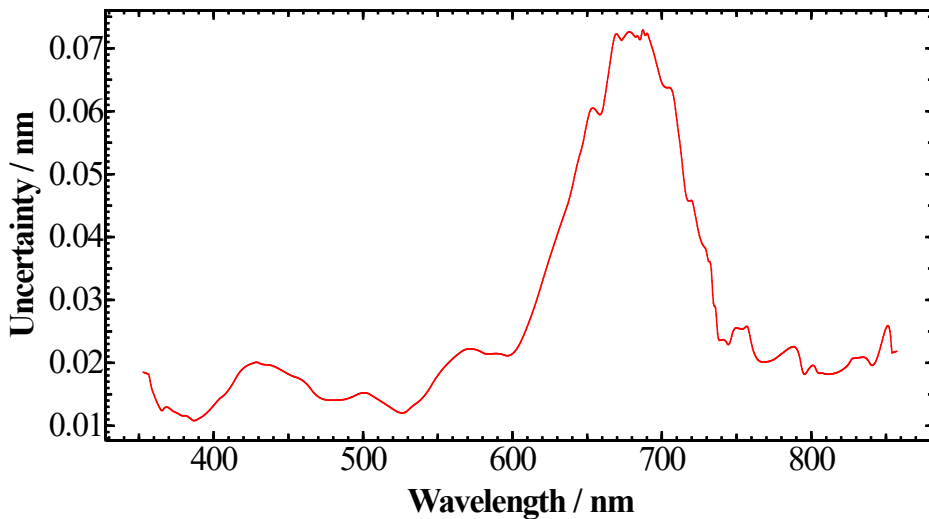


Figure 36. Uncertainty of the wavelength calibration.

Temperature effect

While calibrating and using array spectroradiometers the user must be aware of the temperature effect on the wavelength scale of the instrument. The temperature coefficient can be in the range of several tens of pm / K or even more. Figure 37 shows a change of the wavelength scale of the selected array spectroradiometer when the ambient room temperature is changed from 22 °C to 23 °C. The effect is about 0.02 nm/K.

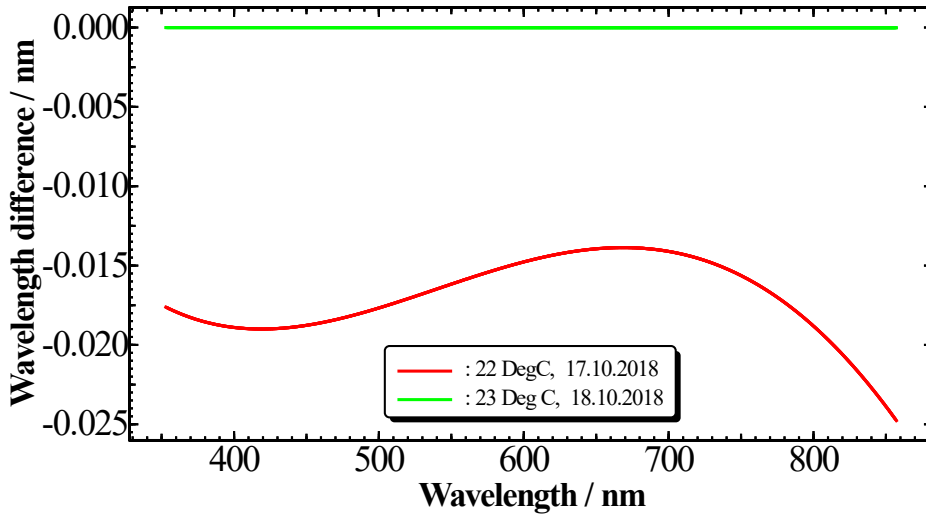


Figure 37. Effect the ambient temperature change on the wavelength scale of the array spectroradiometer.

Instrument stability

The stability of the wavelength scale of an array spectroradiometer may be affected, as demonstrated in Figure 10, by variations of the ambient temperature. The instrument may change its wavelength also as a result of, e.g., a mechanical shock during a transportation. To make sure that the wavelength axis of the array spectroradiometer used for the measurements within the PhotoLED project had not changed in the time slot between the calibration at PTB and METAS, the instrument was calibrated for the pixel-to-wavelength assignment on 18.10.2018, shortly before being taken to METAS for the measurements using a newly developed Fabry-Perot device. Being back to PTB in Braunschweig, it was recalibrated on 30.10.2018. The difference between the two calibrations was in the range between 5 pm to 15 pm (see Figure 11). The minor change in the pixel-to-wavelength assignment may be well explained by the variation of the ambient temperature of the laboratory, which was 23 °C ± 1 °C.

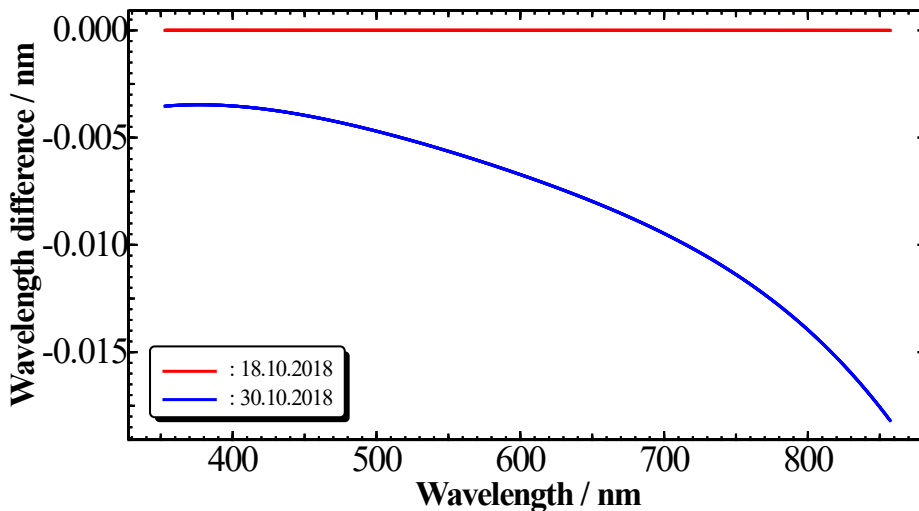


Figure 38. Difference between wavelength scale calibrations of an array spectroradiometer accomplished before and after the transportation from PTB to METAS.

Nonlinearity

Nonlinearity of an array spectroradiometer is a property of the detector system. In general, spectroradiometers with CCD-array detectors may have nonlinearities as high as 10 % and even larger. Thus, this instrumental property requires careful characterisation by radiometric methods that enable then a respective correction to be applied as a function of dark value-subtracted ADC counts. The nonlinearity characterisation of the array spectroradiometers at PTB is done relative to a linear silicon detector by comparing the spectroradiometer signal under irradiation by a laser beam of varying output power to the respective photocurrent values of the linear detector.

The array spectroradiometer type selected for the LED measurements at PTB has a CCD-array detector system with a low nonlinearity. Figure 39 shows the nonlinearity of a spectroradiometer as a function of the ADC counts. The change of the responsivity throughout the dynamic range of the detector is within 2 %. The remaining nonlinearity after the determined correction function is applied is within 0.1 %.

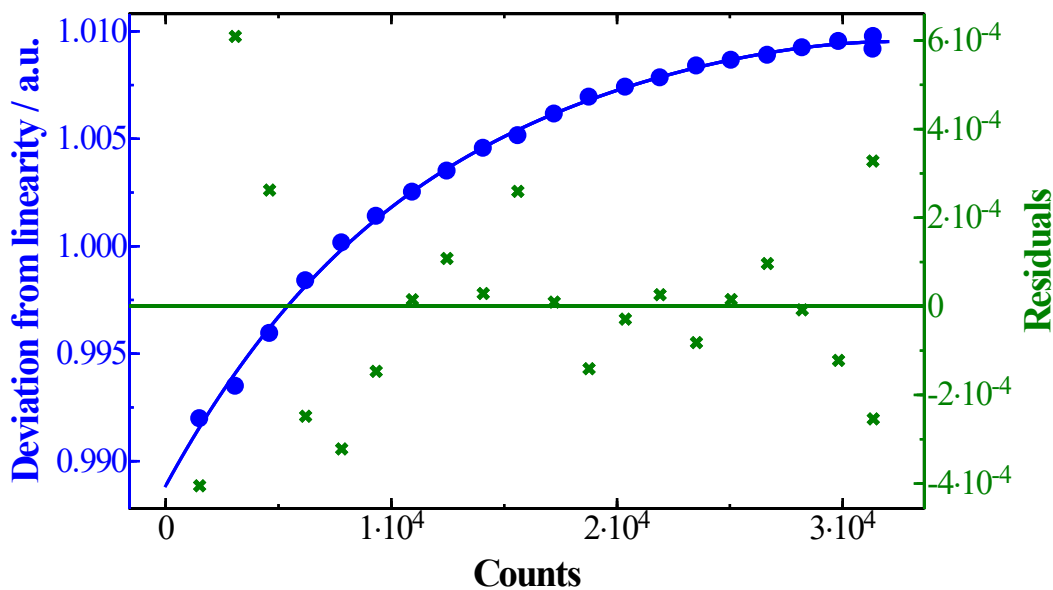


Figure 39: Nonlinearity of a CCD-array spectroradiometer. A 4th-order polynomial was fitted to obtain a correction function for the nonlinearity, which is reduced from 2 % to below 0.1 %.

4.3.3 Comparison of illuminance and validation of luminous intensity of the white LED standards

The presented characterisation methods were used at several NMIs for a comparison of the quantities luminous intensity and illuminance. In the following two figures (Figure 40 and Figure 41) are two LIS-A artefacts shown, which were calibrated with different detector types (photometer, trap and PQED) at NMI partners Aalto, CMI, CSIC, INRIM and PTB.

For these two LIS-A units, the close agreement between the different calibration methods and independent laboratories indicates that the presented calibration methods include the relevant information for corrections and reasonable determination of the measurement uncertainty. This leads to a relative standard uncertainty of 0.31 % (expanded uncertainty $k = 2.025$: 0.64 %) for the luminous intensity calibration of one LIS-A artefact. Results of three of the five partners show very good agreement with measured values within ± 0.2 % of the comparison mean value. Results of two of the five partners show larger deviations, up to 0.5 %, that are related to the unfiltered measurement method. Preliminary examinations of the source for the deviation were carried out and the most probable suspect for the deviation is different flow speed of nitrogen used with the detectors. It was found out that high flow rates cause turbulence in the relatively small entrance aperture of the detector affecting the results. However, further research is needed to determine to which extent this affects the results.

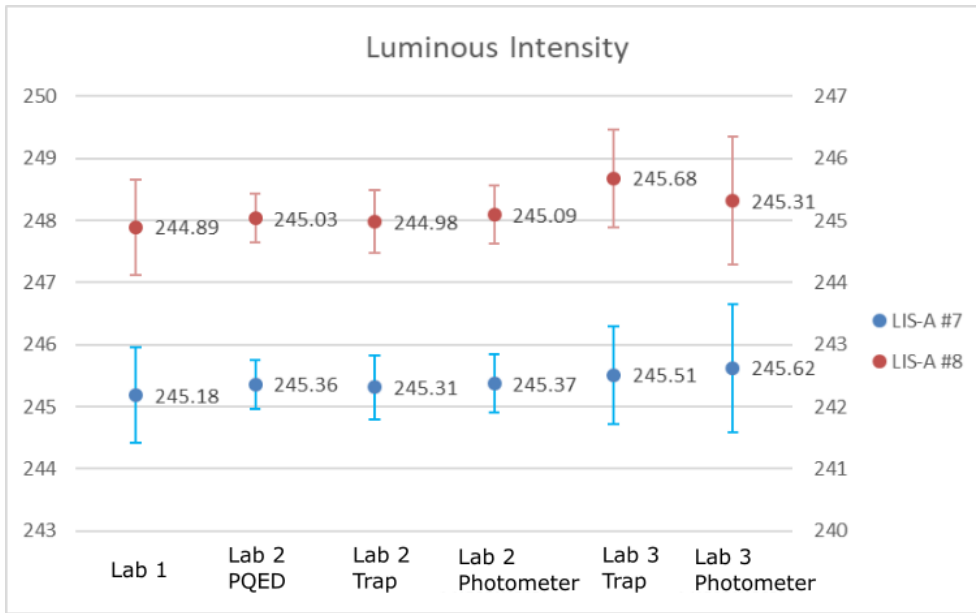


Figure 40: Results of the NMI comparison of luminous intensity values with corresponding standard uncertainties.

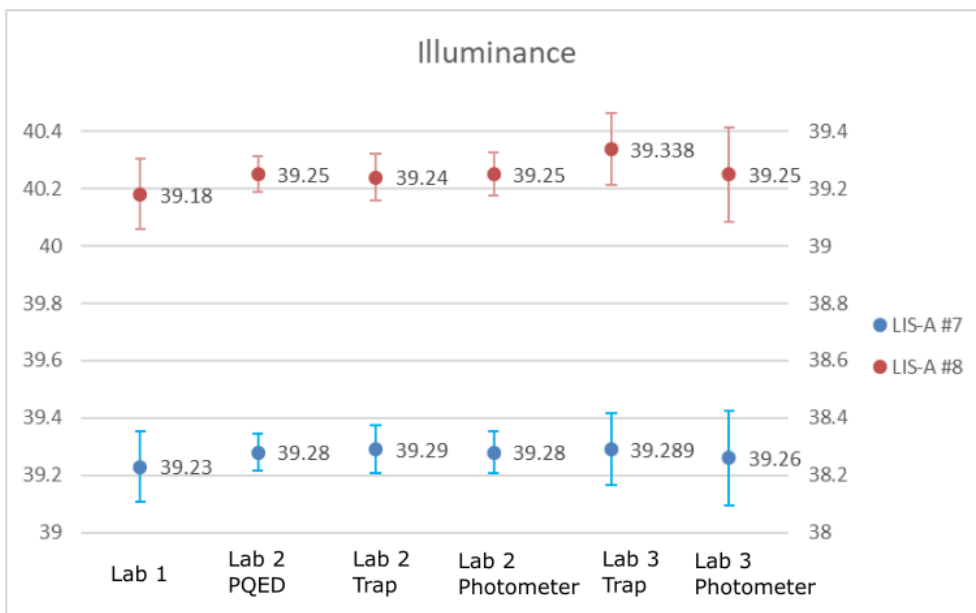


Figure 41: Results of the NMI comparison of illuminance values with corresponding standard uncertainties.

4.3.4 Summary of key research outputs and conclusions

In order to enable NMIs and test laboratories to use LED-based sources for photometric measurements, new photometers were built and thoroughly characterized. The precision apertures for these photometers were manufactured, and then measured using two different methods. The produced detectors were used in the comparison measurements between different NMIs in order to validate the suitability of the newly designed and built LED-based luminous intensity sources. The comparison measurements showed that incandescent standard lamps could be complemented by LED-sources for characterisation of detectors measuring luminous intensity. Results of three of the five partners show very good agreement with measured values within $\pm 0.2\%$ of the comparison mean value. Results of two of the five partners show larger deviations, up to 0.5% , that are related to the unfiltered measurement method. The most probable cause for the deviation is use of different flow speed of nitrogen with the detectors.

4.4 Reducing the uncertainties of luminous flux and luminous efficacy measurement of solid-state lighting (Objective 4)

Due to the phase out of incandescent lighting, testing laboratories increasingly measure SSL products. Luminous flux (lm) and active electrical power consumption (W) of new SSL products coming to market are measured at test laboratories in order to determine the luminous efficacy (lm/W) and energy class of the products. New LED standard lamps with well-defined spectral power distributions (SPDs) and supporting detector technology need to be developed for photometric calibrations at national metrology institutes (NMIs), to provide convenient and reliable traceability for measurements of SSL products to pave the way to lower uncertainties. The introduction of both LED-based reference lamps typically reduces the uncertainties due to spectral mismatch by a factor of 2 on average when measuring SSL products. To facilitate the reduction of uncertainties due to increased variety of angular luminous intensity distribution of modern LED products the easy to implement fisheye camera method has been disseminated to test laboratories and validated. The objective of this work is to reduce the uncertainties of luminous flux and luminous efficacy measurement of solid-state lighting (SSL) products at national metrology institutes to 0.5 % ($k = 2$) and to demonstrate that uncertainties as low as 1 % ($k = 2$) can be achieved in a test laboratory. This objective has been fully achieved.

4.4.1 Fisheye camera method for determining spatial non-uniformity corrections of SSL products in measurements using integrating spheres

When the total luminous flux of a lighting product is measured using an integrating sphere photometer, one of the key sources of uncertainty is the spatially non-uniform responsivity of the sphere. In addition to the uniformity of the integrating sphere itself, this uncertainty stems from disparity of the luminous intensity distributions of the lamp under test and the luminous flux standard lamp used to calibrate the sphere. Before introduction of solid-state lighting to the market, the light sources measured at test laboratories did not vary as much in terms of luminous intensity distributions. Modern LED products, on the other hand, can have very unconventional and application-specific angular distributions.

The uncertainty due to the spatially non-uniform responsivity of the integrating sphere can be up to several percent. This type of uncertainty can be mitigated using the spatial non-uniformity correction, where luminous intensity distribution of the lamp under test is used together with the spatial responsivity map of the sphere to calculate a correction factor for the luminous flux measurement. Traditionally, obtaining the luminous intensity distribution for every lamp under test has required very time consuming and resource intensive goniophotometric measurements.

In this project, a new method was developed to allow easily applying the spatial non-uniformity correction. The method is based on using a fisheye lens camera, installed into a port of the integrating sphere, to determine the luminous intensity distribution of the lamp under test inside the sphere. Using this method, the spatial non-uniformity correction for the luminous flux measurement can be obtained in a matter of minutes without any permanent modifications to existing integrating spheres. Thus, the method enables test laboratories to easily and effectively reduce the measurement uncertainty of the luminous flux and energy efficiency measurements, and also provides the user with the angular distribution of the light source without any extra effort. Figure 42 shows an example of a fisheye camera photograph captured from a port of an integrating sphere, the same image processed using the fisheye camera method algorithm, and the resulting angular intensity distribution.

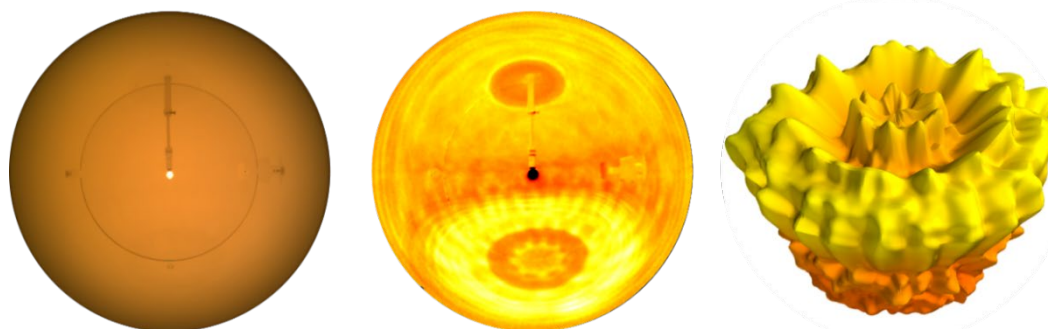


Figure 42. From left to right: fisheye camera photograph, processed fisheye camera image, and obtained angular intensity distribution. Including the installation of the lamp, the measurement procedure took less than a minute.

The collaboration within the project allowed to extensively test and validate the fisheye camera method. In the validation measurements, the method was employed in eight integrating spheres at Aalto, VSL, Signify, DTU, PTB, and OSRAM and compared with the results obtained using five goniophotometers at CSIC, VSL, Signify, CMI, and PTB. The spheres ranged from 1.5 m to 4.0 m in diameter and had various structural configurations and reflectance factors. Figure 43 shows the spatial non-uniformity corrections obtained for six DUTs (devices under test) with eight integrating spheres and five goniophotometers. The maximum difference between the spatial non-uniformity corrections calculated from the luminous intensity distribution measured with a photogoniometer and a fisheye camera was 0.22 %, with the average difference being 0.05 %. This profound validation would have been impossible without the international collaboration in the scope of the project.

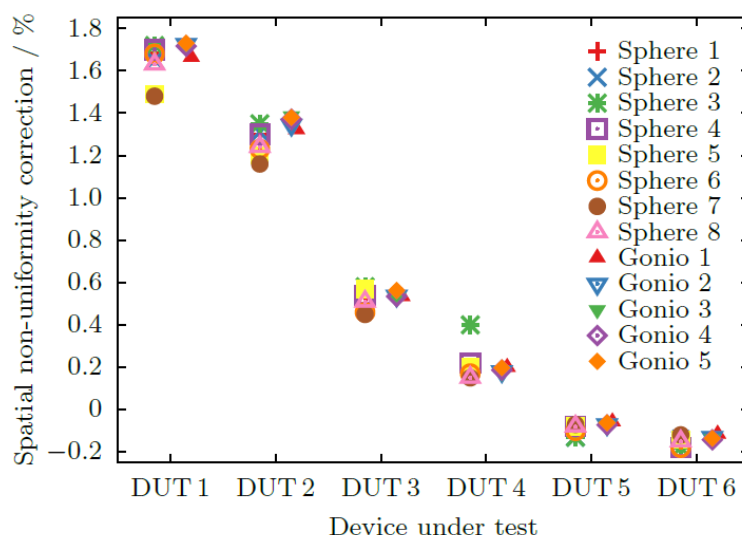


Figure 43. Spatial non-uniformity corrections calculated for the six DUTs and the spatial responsivity map of one sphere using the angular intensity distributions measured with the fisheye camera method in all the eight integrating spheres (left-hand points) and with the five goniophotometers (right-hand points).

Full detail of the validation of the fisheye camera method can be found in:

- Kokka *et al.*, "Validation of the fisheye camera method for spatial non-uniformity corrections in luminous flux measurements with integrating spheres", *Metrologia* **56**, 045002 (2019), DOI: <https://doi.org/10.1088/1681-7575/ab17fe>.

4.4.3 Characterisation of the LED-based luminous flux standard lamps with uncertainty of 0.5 % (k = 2) at the NMI level

Aalto calibrated the luminous flux of the developed DC- and AC-operated LED-based luminous flux lamps. The calibration was based on the absolute integrating sphere method⁵. Lamp to be calibrated was mounted inside a large integrating sphere. External light source (LISA-3, LED-based luminous intensity source developed by PTB) outside the sphere generated a reference luminous flux. The illuminance produced by the external source was measured with a PQED (Predictable Quantum Efficient Detector) photometer at the aperture plane of a precision aperture, approximately 77 cm from the light source. The diameter of the aperture was 40 mm. The reference luminous flux passing through the aperture was obtained by multiplying the measured illuminance with the aperture area. The PQED photometer was removed and the reference luminous flux entered the sphere through an opening on the sphere wall. A signal relative to this reference flux was measured with a photometer attached to the sphere. Another sphere photometer signal was recorded when the lamp under calibration was operated inside the sphere. The ratio of these signals and the known reference luminous flux were used to derive the luminous flux of the lamp under calibration.

The results were fine-tuned by correction factors obtained from the measurement system characterization, which included measurements of several spatial and spectral properties⁵.

⁵ J. Hovila, P. Toivanen, and E. Ikonen, "Realization of the unit of luminous flux at the HUT using the absolute integrating-sphere method," *Metrologia* **41**, 407–413 (2004).

The lamps under calibration were mounted base up to an E27 socket. The AC-operated luminous flux lamps were operated with AC voltage of 230V and the DC-operated lamps were operated with 16 V DC. The lamp was allowed to stabilize for 40 minutes before the calibration measurement started. Then, the luminous flux of the lamp was measured according to the procedure described in Hovila2004, with two exceptions: (1) an LED source was used as the external source instead of a FEL lamp and (2) a PQED without photometric filter in combination with spectral measurement was used instead of the standard photometer when measuring the external source. The voltage and current of the lamp and the photocurrents of the photometers were recorded during the calibration by taking 10 measurement samples with 2-second integration time. The dark currents of the photometers were measured and subtracted from the photocurrents. The spectrum of each luminous flux lamp was measured using Instrument Systems CAS 140 spectroradiometer for calculating a spectral mismatch correction factor. A summary of the calibration results and associated uncertainty budget are given in Table 1 and Table 2.

Table 1. Results of the luminous flux calibration.

Lamp	Luminous flux /lm
P3.1-003	811.8 ± 4.2
P3.1-004	816.1 ± 4.2
P3.1-005	795.4 ± 4.1

Table 2. Uncertainty budget of the calibration.

Component	Relative standard uncertainty / %
<i>Illuminance measurement</i>	
<i>Spectral mismatch correction</i>	
Spectral shape (unknown correlations)	0.13
Extrapolation	0.04
Wavelength scale uncertainty	0.03
Repeatability	0.05
Aperture area (PQED)	0.03
Aperture alignment	0.02
Straylight	0.01
Absolute responsivity at 555 nm	<0.01
Aperture area	<0.01
Distance from detector to aperture (0.3 mm)	0.08
Photocurrent measurement (external)	0.01
Drift of the external source	0.01
<i>Luminous flux measurement</i>	
Drift of the sphere photometer	0.05
Photocurrent measurement	0.02
Beta correction	0.03
<i>Source-related</i>	
Stability of luminous flux	0.15
Spectral mismatch correction	<0.01
Spatial non-uniformity correction	0.10
Combined standard uncertainty	0.26
Expanded uncertainty (k = 2)	0.52

4.4.4 Transfer of the unit of luminous flux to test laboratory level and validation

The AC- and DC-operated reference flux lamps were provided to five test laboratories. After implementing the luminous flux scale on their facility, the test laboratories participated in a round robin. The aim of the round robin was to demonstrate that it is possible to achieve test laboratory uncertainties as low as 1.0 % ($k = 2$) for luminous efficacy. Measurements of luminous flux, active power and luminous efficacy were performed on five AC-operated commercial artefacts and one DC-operated SSL artefact. Five commonly available LED lamps were selected as comparison artefacts covering a range of CCTs (2700 K, 4000 K) and luminous intensity distributions (25° , 2π and 3π). Within the limits of the comparison schedule, some of the participating laboratories used the fisheye camera method for spatial non-uniformity correction, as well as the impedance stabilization network (ISN) for supplying the operating voltage for the product under measurements.

In the round robin, the five testing laboratories measured the sets of five commercial lamps, each using a LED based reference luminous flux transfer standard for their traceability. Each laboratory was able to choose either AC- or DC-operated luminous flux transfer standard based on the power supplies connected to their measurement facilities. Measurements were taken in the sequence co-pilot – NMI – co-pilot – Test laboratory – co-pilot. Both comparison rounds were organized as a star configuration, with each participant measuring a different set of the five lamps and the co-pilot laboratory, RISE measuring all the lamps. The comparison reference value of the lamp sets were determined on the average results of a round robin among NMIs (VSL, CMI, CSIC, METAS and RISE) and the testing laboratories (DTU Fotonik, BFKH, OSRAM, Signify and LMT). The degree of equivalence for luminous flux for all NMIs is better than ± 1 % (see Figure 44).

The lamp sets selected for the comparison among NMIs were used in the comparison among testing laboratories. The degree of equivalence for luminous flux of all test laboratories is shown in Figure 44. For three testing laboratories, the unilateral degree of equivalence was within ± 1 %. This shows that when using LED-based traceability combined with the fisheye camera method for spatial non-uniformity correction, luminous flux measurements can be within agreement of ± 1 %.

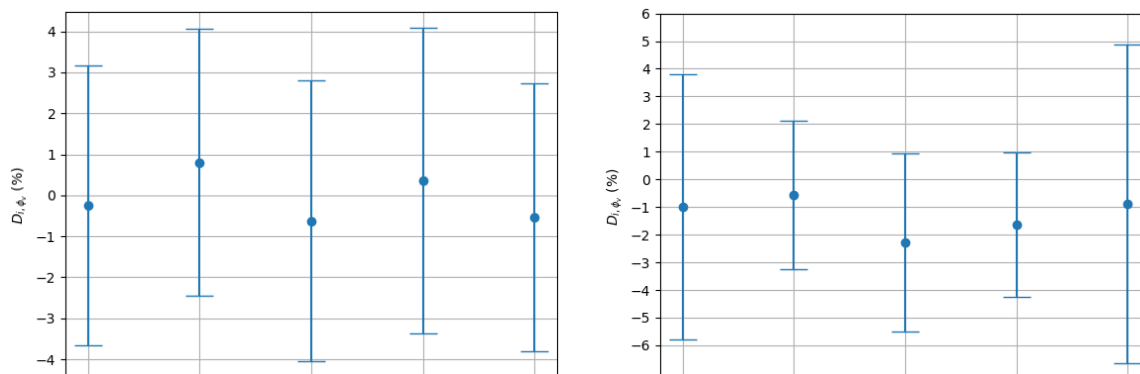


Figure 44. Degree of equivalence of luminous flux in comparisons. Left all NMIs; right: all test laboratories.

4.4.5 Summary of key research outputs and conclusions

To provide traceability to test laboratories with reduced uncertainty, AC- and DC-operated E27-base luminous flux reference lamps based on the 4100 K LED reference spectrum were developed and characterised as transfer standards. Seasoning the lamps for about 800 hours was carried out before using the lamps as transfer standards. After a warmup period of 30 minutes, the short-term luminous flux stability of the lamps is better than 0.1 %. An even better luminous flux stability of 0.01 % can be obtained by extending the warmup period to about 45 minutes. Electronic evaluation of the AC-operated lamps show that the input power variation can be limited to 0.1 % after 2 minutes of stabilization time and the RMS current fluctuation can be limited to 0.1 % instantly. Also, the AC-operated lamps have power factors higher than 0.97 and THD of current lower than 4 %, which facilitates good lamp stability and comparable operation conditions even when different types of AC voltage sources are used. The DC-operated luminous flux standard lamps provide internal thermal control. Without temperature stabilization, the lamps have an average temperature dependence of 0.25 %/°C in luminous flux. In the case of slow temperature fluctuations, such as those originating from the laboratory facility, the temperature controller works as expected, and only a small residual dependence of 0.01 %/°C is observed in the luminous flux. The DC-operated lamp is suitable especially for laboratories, whose laboratory facility is not fully controlled.

To facilitate reduction of uncertainty due to increased variety of angular luminous intensity distribution of modern LED products, the easy to implement fisheye camera method has been disseminated to eight laboratories and validated. As a validation the spatial non-uniformity correction for six DUTs (devices under test) have been determined from the luminous intensity distributions obtained with eight integrating spheres equipped with a fisheye camera and five goniophotometers. The spatial non-uniformity corrections obtained using both methods have been compared. The validation shows that the difference in spatial non-uniformity corrections obtained with the two methods is at maximum 0.22 %, and 0.05 % on average.

Finally, both the dissemination of the luminous flux scale with the AC- and DC-operated reference lamps to test laboratories and the implantation of the fisheye camera method have been validated in a round robin among five test laboratories. Some of the participating test laboratories used the fisheye camera method in their integrating spheres to obtain spatial non-uniformity corrections from the angular luminous intensity distributions of the comparison artefacts. The degree of equivalence for luminous efficacy of three of the five test laboratories was within 1 %. The degree of equivalence of all five test laboratories was well within their claimed uncertainty. The uncertainties of some participating laboratories were limited due to the tight schedule of the comparison. As a result, not all laboratories could utilize the fisheye correction, or the ISN in their measurements. This shows that the uncertainties claimed can likely be reduced when using the LED-based transfer standard, proper spatial non-uniformity correction, and impedance stabilization. Partly this reduced uncertainty is attributed to reduced spectral mismatch errors stemming from the LED-based spectral distributions both in calibration of the luminous flux scale and in measurements of the commercial SSL products.

5 Impact

Prior to the development of the LED calibration spectra and standard lamps, a stakeholder workshop was organised in May 2017 at METAS, Switzerland to gather input from CIE and industry. The workshop was arranged during the CIE Tutorial and Practical Workshop on LED Lamp and Luminaire Testing to CIE S025 with a total of 36 participants from test laboratories, instruments manufacturers and people working in CIE TCs. The project participated actively in the CIE 2017 Midterm Meeting on Jeju, Korea in October 2017 by providing 5 presentations and 1 poster on topics related to the new LED illuminants, LED reference spectrum and the new measurement methods under development. In addition, a two-hour workshop and a dedicated meeting was arranged with a total of 30 participants, to agree the start of a new technical committee within CIE, for defining the LED reference spectrum.

The first PhotoLED training session was arranged for the EURAMET TC-PR members in their annual meeting at IPQ, Portugal on 29 January 2019. During this session, the standard lamps for luminous intensity and luminous flux were presented with possibility to operate the lamps by the participants. Additionally, several presentations were given about the results of the project. The project partners presented 7 talks and 2 posters in the CIE 29th Quadrennial Session in Washington DC, USA, in June 2019, including topics covering the development of the new LED standard lamps, validation of the fisheye camera method, definition of photometric quality index and application of LED illuminants in analysis of colour graphic icon for real complex scenes.

In August 2019, the project arranged a key stakeholder event at DTU Fotonik in Roskilde, Denmark. The event consisted of a technical workshop with presentations and a discussion, as well as a hands-on laboratory training session with the light sources and measurement methods developed in the project. The event gathered approximately 25 people from the industry, universities and companies. The topics covered by the workshop and the training included measurement of the illuminance and luminous intensity of the luminous intensity standards LIS-A using unfiltered detectors with nitrogen flow, the fisheye camera method for spatial correction with an integrating sphere and the two luminous flux standard lamps.

Impact on industrial and other user communities

This project successfully investigated new methods to change the way how the lighting industry will utilise photometry in the future. The project demonstrated that classical tungsten filament standard lamps can be replaced by standard lamps based on LED technology that will reduce the spectral errors in measurements of SSL products to 1/2, reduce the stabilisation time and signal noise, offer better stability, robustness and lifetime, for maintaining photometric scales in laboratories and shipping of the lamps between NMLs and test laboratories.

Achieving lower uncertainties in photometric measurements of SSL products benefits the lighting industry and consumers. Once the methods are widely taken into use, manufacturers of SSL products will be better able to

rely on the measurement results from test laboratories, thus speeding up product development and enabling better judgement of the performance of new products coming to market. With the development of a coherent and efficient European metrological infrastructure based on LED-based photometric standards, new measuring instruments and supporting measurement methods, as well as written standards, the benefits of SSL products such as energy efficiency, will be assured and market penetration will be increased.

Impact on the metrology and scientific communities

This project has contributed to solving the metrological problems caused by phasing out of incandescent standard lamps, and has been leading the investigation of an improved scientific and technical system of photometry for the measurement of LEDs and other SSL products for the benefit of the society, which better reflects the characteristics and requirements of these type of lighting products.

Impact on relevant standards

This project has been involved in the work of several CIE TCs to update the existing standards and technical reports which describe the recommended methods used in photometry and colorimetry. The development of the new LED illuminants and LED reference spectrum has been carried out with close connections to CIE since the start of the project, with both Division 1 and 2 included in the discussions. The project has been actively communicating with CIE TC1-85 related to the development of the new LED illuminants. These illuminants are now included in the revision of the CIE15: Colorimetry, 4th Edition, enabling colorimetric calculations with LED spectra of different types. The project partners have participated in many TCs of CIE Division 2 to ensure that the introduction of new physical LED standard lamps and supporting measurement methods, including the fisheye camera method, are included in these technical documents. In June 2018, a new CIE Division 2 Technical Committee TC2-90 'LED reference spectrum for photometer calibration' was established to further analyse and publish the LED reference spectrum as a CIE Technical Report. Once the document has been published, commercial LED standard lamps can be manufactured with CIE recommended reference spectrum to complement the Standard Illuminant A in photometer calibrations.

Longer-term economic, social and environmental impacts

The results of the project will enable more reliable classification of energy efficiency of lighting products based on SSL technology. When new technologies reach the market, the consumer will have better confidence in the stated performance of the products, i.e. the values printed on the box, thus enabling them to make more informed choices. A sound metrological framework is the backbone of all accurate measurements. Low uncertainties obtained by high quality measurements increase the confidence in the products and enable better differentiation between the characteristics of various products. Achieving lower uncertainties in the testing of SSL products will also result in less waste and reduced costs for manufacturers due to fewer SSL products being erroneously rejected from entering the market because of the use of large guard bands in determining the energy classes of products.

6 List of publications

- [1] A. Kokka, T. Poikonen, P. Blattner, S. Jost, A. Ferrero, T. Pulli, M. Ngo, A. Thorseth, T. Gerloff, P. Dekker, F. Stuker, A. Klej, K. Ludwig, M. Schneider, T. Reiners and E. Ikonen, “Development of LED illuminants and reference spectrum for colorimetry and photometry”, *Metrologia* **55**, 526–534 (2018). <https://doi.org/10.1088/1681-7575/aacae7>
- [2] A. Ferrero, J.L. Velázquez, A. Pons, and J. Campos, “Index for the evaluation of the photometric performance of photometers”, *Opt. Express* **26**, 18633–18643 (2018). <https://doi.org/10.1364/OE.26.018633>
- [3] Y. Zhu, “Development of Transfer Standards for SSL Measurement”, Master’s thesis (Delft University of Technology, Netherlands, 2017). <http://resolver.tudelft.nl/uuid:dd6df3c3-fb96-4fbe-8cfe-56d664d2d9b4>
- [4] A. Kokka, T. Pulli, T. Poikonen, J. Askola, and E. Ikonen, “Fisheye camera method for spatial non-uniformity corrections in luminous flux measurements with integrating spheres”, *Metrologia* **54**, 577–583 (2017). <https://doi.org/10.1088/1681-7575/aa7cb7>
- [5] A. Kokka, T. Pulli, Alejandro Ferrero, Paul Dekker, Anders Thorseth, Petr Kliment, Adam Klej, Thorsten Gerloff, Klaus Ludwig, T. Poikonen, and E. Ikonen, “Validation of the fisheye camera method for spatial non-uniformity corrections in luminous flux measurements with integrating spheres”, *Metrologia* **56**, 045002 (2019). <https://doi.org/10.1088/1681-7575/ab17fe>
- [6] A. Kokka, “Spatial and Spectral Corrections for Integrating Sphere Photometry and Radiometry”, Doctoral dissertation, Aalto University (2019). <https://aaltodoc.aalto.fi/handle/123456789/37563>